MINISTRY OF DEFENCE

AERONAUTICAL RESEARCH COUNCIL

REPORTS AND MEMORANDA

An Application of the R.A.E. Wind-Tunnel/ Flight Dynamics Simulator to the Low-Speed Dynamics of a Slender Delta Aircraft (HP 115)

by D. W. PARTRIDGE and B. E. PECOVER

Aerodynamics Dept., R.A.E. Farnborough

An Application of the R.A.E. Wind-Tunnel/ Flight Dynamics Simulator to the Low-Speed Dynamics of a Slender Delta Aircraft (HP 115)

by D. W. Partridge and B. E. Pecover

Aerodynamics Dept., R.A.E. Farnborough

Reports and Memoranda No. 3669*
August, 1969

Summary.

The wind-tunnel/flight dynamics simulator has been applied to a limited study of the dynamic response at low speeds of the Handley-Page HP 115 aircraft. Motions with six degrees of freedom were simulated. The technique provides full representation of the non-linearities in the aerodynamic force and moment contributions due to translational velocity components.

Good qualitative agreement with flight test results was achieved. The amplitude damping characteristics of the Dutch roll oscillatory motion appear to be largely dependent on the translational velocities.

LIST OF CONTENTS

1. Introduction.

The Handley-Page HP 115 is a slender-delta research aircraft built to investigate the low-speed handling properties of aircraft having slender delta wings. The aircraft is shown in Fig. 1, and a detailed description is given in Ref. 1. Flight tests have shown[1] the Dutch roll mode of the aircraft to be stable at incidences below 18°, but to diverge gently to a sustained oscillation at higher incidences.

The wind-tunnel-flight dynamics simulator[2] is a facility primarily designed to investigate the behaviour of vehicles at high Mach number, where the static aerodynamics, i.e. those due to translational velocity components only, predominate. The wind tunnel acts as a function generator for the static aerodynamic forces and moments. This information, together with vehicle mass, inertia, and dynamic aerodynamic derivatives is supplied to an on-line computer which solves the Euler equations of motion of the vehicle. The computed solutions are used to control the orientation of the model to the tunnel airstream. Thus an accurate representation of the translational velocity aerodynamics is maintained throughout the simulation. The angular velocity aerodynamic force and moment contributions are included by utilising the rotary derivatives as estimated or independently measured and generating the associated forces and moments in the computers in a manner similar to that of conventional simulation technique. The facility utilises the R.A.E. No. 19 supersonic wind tunnel.

Probably because an adequate mathematical model of the aerodynamics has not been devised, a fully representative simulation of the HP 115 Dutch roll has not been achieved by conventional simulators. In addition to providing insight into the mechanisms of the Dutch roll, the present simulation has provided a particularly stringent test of the flight dynamics simulator performance.

The tunnel was modified to give subsonic flow in the working section by installing a choked second throat downstream of the working section. Tests commenced with the aircraft trimmed at incidence. The Dutch roll oscillations were either allowed to build up naturally, or were triggered by a yawing moment disturbance. Full six degrees of freedom were represented. The effects of variations of the rolling moment magnitude, and of the dynamic derivatives were briefly studied. Despite the fact that the model used was considerably less representative than the normal standard of models used with the simulator (*see* Section 2), qualitative agreement with the flight tests was achieved.

2. Model.

Models for the flight dynamic simulator wind tunnel are usually made as geometrically representative as possible, in the interests of obtaining truly representative aerodynamic characteristics. They are usually equipped with remotely operable control surfaces, since these increase the range of simulations possible, because they provide bonuses of accuracy, and because by avoiding tunnel shut-downs between runs, they enable a given test programme to be completed in a shorter time.

Since the tests proposed for the present model were of restricted scope, and only qualitative agreement with flight records was sought, it was decided, with a view to getting a model quickly, to accept a less sophisticated model lacking the above amenities.

The 1/40 scale model has been simplified by using a wing and fin of double wedge section instead of the correct biconvex (the same thickness/chord ratio being retained) and by the omission of the nose probe and parachute fairing. No attempt has been made to represent the elevon hinge gap and the rear-body has been distorted in order to accommodate an existing six-component internal strain-gauge balance. The flow through the engine has not been represented and the intake has been closed by a conical fairing. The model is shown in Figs. 2 and 3.

Three alternative elevons were available with fixed settings of $\eta = 0°$, $-7\cdot5°$ and $-15°$. Apart from some check tests, the $-7\cdot5°$ elevons were used throughout.

3. Wind Tunnel.

The R.A.E. No. 19 wind tunnel, which has heretofore been used for supersonic tests only, was converted to subsonic operation for the purposes of the simulations described herein. A choked second throat technique was used to enable the tunnel to be operated at a predetermined subsonic Mach number, independently of minor compressor performance variations. This technique also effectively insulates

the working section flow from disturbances which would otherwise be propagated upstream from the diffuser, cascades etc. and this provides a smoother (less 'noisy') flow. So long as sufficient pressure ratio is maintained to choke the second throat the working section Mach number then depends only on the ratio of the areas of the second throat and working section (neglecting viscous effects). A continuously variable second throat is under construction, but for these tests this area ratio was fixed and designed to give a nominal $M = 0.3$. In this configuration it was found that the second throat was choked even with the finest compressor blade-angle setting available. Upstream of the working section the nozzle for the lowest supersonic Mach number (1.4) was employed, since this had a throat substantially larger than the second throat and provided some allowance for boundary-layer growth in the working section.

Calibrations of Mach number and flow direction were made in the presence of the support gear but without the model. Pitot-static and four-hole yaw-meter probes mounted on the tunnel traverse gear were employed for this purpose and some typical results are given in Figs. 4 and 5. These show the Mach number variation to be ± 0.004 from a mean 0.297, the Mach number falling progressively from upstream to downstream. The flow direction diverges vertically from the tunnel axis by $0.1°$ per inch of height. The lateral component of flow direction exhibits only small changes.

In order to ensure that the working section flow was not subject to gross changes such as might be caused by wall separations provoked by the model and/or support attitude, further pitot/static traverses were made with the support attitude varied with and without the model present and with its attitude also varied. In particular points close to the edge of the tunnel boundary layer were examined. There was no evidence of any variation in boundary-layer thickness due to variations in model and support attitude.

4. Translational Velocity Aerodynamic Forces*.

These are the aerodynamic force and moment contributions arising from the magnitude and direction of the relative wind velocity vector, in the absence of any rotational velocity or time dependence. The relative wind velocity vector can be resolved into components, u, v, w along the datum body axes, and these may then be normalised by the resultant velocity to $\bar{u}$, $\bar{v}$, $\bar{w}$. It will be noted that $\bar{v}$ and $\bar{w}$ are related to generalised forms of the sideslip and angle of attack respectively reducing to the conventional forms for small values of these velocities. Figs. 6 to 11 show the variation of the force and moment components with $\bar{v}$ and $\bar{w}$ for the elevon deflection used in the simulations $\eta = -7.5°$.

The longitudinal data are presented as coefficient *versus* $\bar{w}$ for discrete values of $\bar{v}$, including one negative value. The roll data are given as C_l *versus* $\bar{v}$ for discrete values of $\bar{w}$ and the directional data are in carpet plot form. No corrections for tunnel blockage or constraint effects have been included but $\bar{v}$ and $\bar{w}$ have been automatically compensated for sting bending.

An important feature of the results is the large variation in rolling-moment coefficient, C_l, at a given non-zero $\bar{v}$ with change of $\bar{w}$. The yawing-moment coefficient, C_n, variation with $\bar{v}$ is also markedly non-linear.

Other measurements of HP 115 translational velocity aerodynamics have been made previously by Engler and Moss[3], using a much more representative model in the 13ft × 9ft tunnel at R.A.E., Bedford, and by Thompson, Fail and Inglesby[4], also in the 13ft × 9ft tunnel, but using a different model and support rig. Some of the results of these other tests have been transferred to body datum axes where necessary and plotted with the present results in Figs. 6 to 11 for comparison. It can be seen that the results of the present tests, using the simplified model, are very similar qualitatively to the earlier results, so that the primary aim has been met. There are, however, quantitative discrepancies, some of which are greater than anticipated. In particular the C_z slope measured in these tests was some 22 per cent larger than in the results of Engler and Moss. Appendix A describes the endeavour which has been made to identify the sources of this discrepancy.

---

*This description is used in place of the commonly used, but somewhat contradictory, term 'static aerodynamics' which is particularly inappropriate in the present dynamic connotation. Some such term is required to identify these loads.

A reconciliation is possible with the C_z results of Thompson, Fail and Inglesby by taking account of the measured effect of wing-section and the calculated tunnel-constraint incidence correction. The remaining difference could possibly be attributable to the omission of the elevon hinge gap.

5. *Angular Velocity Aerodynamics.*

These cover all the aerodynamic contributions to the forces and moments not measured directly on the model in the wind tunnel and include those defined by the derivative coefficients $C_{lp}\,C_{mq}\,C_{nr}\,C_{lr}\,C_{np}$ C_{yp}. The estimated values were taken from flight test results[1] and the wind-tunnel test rig results of Thompson and Fail[5].

The dependences on angle of attack $\alpha(\equiv \sin^{-1} \bar{w})$ have been included in the form $a + b\,\bar{w} + c\,\bar{w}^2$ where a, b and c are constants. Fig. 12 shows a comparison between the flight results, tunnel results and the values used for the simulations. The fit achieved is well within the limits of experimental error of the sources.

The derivative coefficients $C_{m\bar{w}}$ and $C_{n\bar{v}}$ were not included in the simulation as reliable estimates were not available. Over the range of incidence studied, their effect was not expected to be large.

6. *The Computer Program.*

The full six degrees of freedom motions were included in the simulation. The contributions of engine thrust were included.

The aerodynamic forces and moments were measured along and about an aircraft datum body axis system. As this system was angularly displaced about the $0y$ axis relative to the principal body axes, the Euler moment equations include product of inertia terms. The equations of motion are

$$\dot{u} = X/m + n_1\,g - q\,w + r\,v + T_X/m$$

$$\dot{v} = Y/m + n_2\,g - r\,u + p\,w$$

$$\dot{w} = Z/m + n_3\,g - p\,v + q\,u + T_Z/m$$

$$I_{XX}\,\dot{p} = L + (I_{YY} - I_{ZZ})\,q\,r + I_{XZ}\,(\dot{r} + p\,q)$$

$$I_{YY}\,\dot{q} = M + (I_{ZZ} - I_{XX})\,r\,p + I_{XZ}\,(r^2 - p^2)$$

$$I_{ZZ}\,\dot{r} = N + (I_{XX} - I_{YY})\,p\,q + I_{XZ}\,(\dot{p} - q\,r)$$

$$\dot{n}_1 = n_2\,r - n_3\,q$$

$$\dot{n}_2 = n_3\,p - n_1\,r$$

$$\dot{n}_3 = n_1\,q - n_2\,p$$

where $X\,Y\,Z$ are the aerodynamic forces

      $L\,M\,N$ are the aerodynamic moments

      $u\,v\,w$ are the components of translational velocity of the *cg* relative to the earth, along the body axes

      $p\,q\,r$ are the components of angular velocity of the aircraft relative to the earth, about the body axes

      $n_1\,n_2\,n_3$ are the direction cosines of the body axes relative to the vertical earth axis

      m is the aircraft mass

      $I_{XX}\,I_{YY}\,I_{ZZ}$ are the moments of inertia about the body axes

      I_{XZ} is the product of inertia

g is the acceleration due to gravity

T_X T_Z are components of engine thrust along the datum body axes

The required orientation of the aircraft to the flight path (corresponding to the model attitude in the wind tunnel) is computed from

$$\bar{v} = v/V$$

$$\bar{w} = w/V$$

where $V = (u^2 + v^2 + w^2)^{\frac{1}{2}}$.

The aerodynamic forces and moments used in the simulation were

$$X = X(\bar{v}, \bar{w})$$

$$Y = Y(\bar{v}, \bar{w}) + \rho\, VS\, l_2\, p\, C_{Yp}\,(\bar{w})$$

$$Z = Z(\bar{v}, \bar{w})$$

$$L = L(\bar{v}, \bar{w}) + \rho\, VS\, l_2^2\, p\, C_{lp}\,(\bar{w}) + \rho\, VS\, l_2^2\, r\, C_{lr}\,(\bar{w})$$

$$M = M(\bar{v}, \bar{w}) + \rho\, VS\, l_1^2\, q\, C_{mq}\,(\bar{w})$$

$$N = N(\bar{v}, \bar{w}) + \rho\, VS\, l_2^2\, r\, C_{nr}\,(\bar{w}) + \rho\, VS\, l_2^2\, p\, C_{np}\,(\bar{w})$$

where $X(\bar{v}, \bar{w})$, $Y(\bar{v}, \bar{w})$, $Z(\bar{v}, \bar{w})$, $L(\bar{v}, \bar{w})$, $M(\bar{v}, \bar{w})$, $N(\bar{v}, \bar{w})$ are the aerodynamic force and moments derived from measurements made directly in the wind tunnel. C_{yp}, C_{lp}, C_{lr}, C_{mq}, C_{nr}, C_{np}, are prescribed functions of $\bar{w}$ generated in the computer outside the wind tunnel (*see* Section 5).

ρ is the air density

S is the wing area

l_1 is the root chord

l_2 is the semi-span

The characteristics of the aircraft are given below

$$I_{XX} \quad 2182 \text{ kg } m^2$$
$$I_{YY} \quad 23517 \text{ kg } m^2$$
$$I_{ZZ} \quad 25430 \text{ kg } m^2$$
$$I_{XZ} \quad 1615 \text{ kg } m^2$$
$$m \quad 2154 \text{ kg}$$
$$S \quad 40\cdot18 \ m^2$$
$$l_1 \quad 12\cdot192 \ m$$
$$l_2 \quad 3\cdot048 \ m$$
$$T_X \quad 7123 \ N$$
$$T_Z \quad -356 \ N$$

7. *Test Procedure.*

An altitude of 3000 *m*, which proved convenient for the simulator program and at the same time realistic for comparison with flight data, was used for all simulations.

Because of the absence of servo controlled elevators on the model, all tests were ultimately carried out using the $7\frac{1}{2}°$ elevator setting. The effect of elevator angle change was simulated by off-setting the zero of the pitching moment measurement channel. Any secondary aerodynamic contributions due to elevator deflection were not therefore reproduced.

The maximum inclination between the model longitudinal axes and the flow direction available in the tunnel is 25°. Thus oscillations were restricted to those which did not involve simultaneously large angles of attack and sideslip. This did not prove a serious limitation, however, as the region of interest where the damping was zero was around 12° incidence.

In order that the airspeed and incidence changes during the Dutch roll simulations should remain small, it was necessary to commence each test with the longitudinal forces and moments trimmed. Out-of-balance forces caused a very lightly damped low frequency motion of period of about 35 seconds. The procedure adopted was to carry out a preliminary test at each incidence to determine the trim values of airspeed and body axis orientation to the earth (n_1). The model was set at incidence and the pitching moment trimmed out. Simulation was then allowed to proceed. The resulting plots of air-speed and n_1 were inspected to determine the trim values to be set in the computer for the start of the test.

In cases where the Dutch roll motion was divergent it proved unnecessary to provide any initial excitation. For stable cases, a pulse of yawing moment was applied to excite the mode. In the absence of a servo-operated rudder, this was most conveniently achieved by momentarily disturbing the yawing moment strain gauge balance. This imposed on the on-line data correction unit an input which was not in accordance with the calibration and hence small disturbances arose on the other force and moment channels exciting the longitudinal oscillatory motions.

The responses were plotted at several values of incidence in the range corresponding to $\bar{w} = 0.1$ to $\bar{w} = 0.24$ (i.e. approximately 6° to 14°). For each test $\bar{v}$, $\bar{w}$, n_1, V, r and bank angle were plotted against time. At $\bar{w} = 0.24$, the effect of varying the magnitude of C_l and of the derivatives C_{lr}, C_{np} and C_{yp} were investigated.

8. *Results.*

The purpose of the experiment had been to examine the applicability of this particular simulation technique in demonstrating for this aircraft response characteristics which had been obtained in flight but which had eluded other more conventional forms of simulation. Because the wind-tunnel model was not fully representative of the full scale aircraft, complete quantitative agreement was not to be expected. The quest was for the reproduction of flight trends, particularly as regards a limit cycle in the Dutch roll motion. In the event, good qualitative agreement was obtained, all the flight trends being reproduced by the simulator.

The lateral motion of the model was observed for flight conditions covering a range of 'trimmed' conditions corresponding to the range of values of $\bar{w}$ from 0.1 to 0.24 (i.e. an angle of attack range of approximately 6° to 14°).

Fig. 13a shows the $\bar{v}$ and $\bar{w}$ histories following an excitation of the lateral motion by means of a yawing moment pulse from a trimmed angle of attack corresponding to approximately $\bar{w} = 0.11$. At this modest angle of attack the Dutch roll motion is well damped and coupling of the lateral and longitudinal motion is only significant during the early stages of the response.

When the trimmed value of $\bar{w}$ is raised to about 0.14 the Dutch roll motion is very lightly damped as can be seen from the curve of $\bar{v}$ in Fig. 13b. The abrupt change of amplitude in the $\bar{v}$ trace corresponds to the application of a yawing moment pulse. It is interesting to compare these results with those shown in Fig. 13c, which refer to practically the same trimmed flight condition. In this latter test, however, the initiating input into the system is such that the response in the angle of attack (or strictly $\bar{w}$) exhibits more variation with time, containing not only the small amplitude oscillation of double the Dutch roll frequency, but also an oscillation of low frequency. These changes in $\bar{w}$ are reflected in the $\bar{v}$ response in that the damping of the Dutch roll motion, which the results in Fig. 13b show to be marginal at this trimmed condition, can move through its zero value leading to sustained oscillations in $\bar{v}$, whose amplitude waxes and wanes slightly according to the value of $\bar{w}$.

The results at a trimmed value of $\bar{w}$ of about 0.195 shown in Fig. 13d are of interest as they not only

7

show the same sustained oscillation of $\bar{v}$, but also quite clearly the effects of the aerodynamic and kinematic coupling terms on the $\bar{w}$ response. Fig. 13c refers to a somewhat larger trimmed angle of attack (or $\bar{w}$). In this instance it was unnecessary to provide an initiating yawing moment and the $\bar{v}$ diverges from zero to amplitudes of the order of 0·1. During the initial phase of this response the variation in $\bar{w}$ is very slight, but when the amplitude of $\bar{v}$ becomes appreciable, there are the expected fluctuations in $\bar{w}$, arising from the non-linear coupling terms in the equations of motion. These again influence the response in $\bar{v}$ which beyond about 40 sec seems to become almost constant in amplitude for the few remaining swings shown on the record.

The oscillations about a slightly larger value still ($\bar{w} = 0\cdot24$) are shown in Fig. 13g. The history of $\bar{v}$ starts off again as a divergent oscillation, the amplitude of which grows throughout the period of time covered, but there is a suggestion that the amplitude may become more or less steady at around 0·2. This completes the series of results chosen to illustrate the effect of the trimmed flight condition on the six-degree-of-freedom motion of the aeroplane. These indicate that below some angle of attack the motion damps out at a rate which decreases as the trimmed angle of attack is increased. Beyond a certain value of $\bar{w}$, that is, above a certain angle of attack, the motion is unstable at small amplitude and so diverges until it reaches a certain amplitude, when it takes the form of a more or less sustained oscillation. The amplitudes of the variable $\bar{v}$ in this latter case are sufficient to produce significant responses in $\bar{w}$, the nature of which reflects the two coupling terms, one kinematic and the other aerodynamic, which give rise to it.

In the limited time available it was not possible to make a thorough investigation of the effect of varying each contribution to the aerodynamic forces and moments in turn on the motion. Also no attempt was made to obtain a closer quantitative agreement with flight test data by this means, but some modifications to the aerodynamic forces and moments were made and their effects noted. The damping derivatives C_{lp}, C_{nr} and C_{nq} have a marked effect on the lateral and longitudinal motions, whilst changes in C_{yp}, C_{lr} and C_{np} have little noticeable effect.

It is to be expected that the strong influence of angle of attack on the rolling and yawing moments arising from the translational velocities (i.e. $L(\bar{v},\bar{w})$ and $N(\bar{v},\bar{w})$) play an important role in the 'Dutch roll' motion arising in the general six-degree-of-freedom motion. Accordingly three tests were made, in which the magnitude of $L(\bar{v},\bar{w})$ was adjusted by varying the gain of the rolling moment measurement channel. In all three tests the initial conditions were identical. The trimmed value of $\bar{w}$ is about 0·24 and at this value the motion in $\bar{v}$ diverges in the manner previously discussed. Fig. 14a shows the results corresponding to the unmodified rolling moment contribution, whilst Figs. 14b and c refer to a 10 per cent and 25 per cent reduction in the rolling moment. In these results there is definite evidence of a sustained oscillation in the $\bar{v}$, the amplitude of which decreases as the rolling moment contribution due to the translational velocities is reduced.

In a subsequent analytical study of non-linear dynamic systems, Beecham and Ross[9] have applied a new technique to the study of the sustained oscillations exhibited in the present tests. Using the same numerical values of the angular velocity derivatives (Section 5), they predict the existence of these sustained oscillations and their quantitative dependence upon the angle of attack, and show the behaviour to be explicable in terms of the non-linearity of $N(\bar{v},\bar{w})$ with $\bar{v}$.

A simulated recovery from a limiting Dutch roll oscillation is shown in Fig. 15. The traces are a complete set of simulator motion parameter time histories during and prior to recovery. The test was started with the aircraft trimmed at high angle of attack, and the Dutch roll allowed to build up until the amplitude approached the limiting value. Recovery was effected by changing the simulated elevator setting to a value corresponding to a lower, stable, angle of attack. The time histories of the roll angle and the yaw rate may be genuine arising from the excitation of the other modes, or may be due, at least in part, to drifts in the corresponding moment measurement channels.

A comparison of 'roll/yaw' ratio* and period with flight is given in Fig. 16. The period shows close agreement. The magnitude of the roll/yaw ratio differs, but the trend with C_L is similar.

---

* Roll-yaw ratio is defined here as amplitude of $\int p\,dt$ ÷ amplitude of $\bar{v}$.

The incidence at which the Dutch roll damping becomes zero is much lower on the simulator than in flight—approximately 12° compared with 18°. This is probably due to differences between the C_Z and C_l obtained with the present model and in flight. The values of C_Z obtained with this model are larger than those measured on a more representative model in the 13ft × 9ft tunnel.[3] Aeroelastic effects such as the control linkage flexibility which exists in the aircraft could reduce the rolling moments obtained in flight. Such effects could be simulated with a more refined model and programme.

9. *Conclusions.*

The sustained amplitude, Dutch roll mode of the HP 115 aircraft has been successfully simulated in the wind-tunnel flight-dynamics simulator. The main purpose of the limited experiment has thus been fulfilled in that good qualitative agreement with flight behaviour has been achieved in conditions where non-linearities, aerodynamic and dynamic, are significant. It is clear that, had the terms of reference so justified, a more penetrating study could have profitably been made. Even so, the limited tests with a comparatively crude model have served to show up the importance of the contribution to the rolling moment from the translational velocities in the development of the sustained oscillations.

9

LIST OF SYMBOLS

b	Semi span of gross wing of the model (76·2 mm 3·00 in)
C	Tunnel working section cross section area (0·209 m^2 324 in^2)
c	Centreline chord of the gross wing of the model (304·8 mm 12·00 in)
C_l	Rolling-moment coefficient non-dimensionalised on $q\,S\,l_2$
C_m	Pitching-moment coefficient non-dimensionalised on $q\,S\,l_1$
C_n	Yawing-moment coefficient non-dimensionalised on $q\,S\,l_2$
$C_X\,C_Y\,C_Z$	Force coefficients non-dimensionalised on $q\,S$
$C_{lp}\,C_{lr}$	Derivative coefficients of rolling moment due respectively to roll rate and angular velocity in yaw, non-dimensionalised on $\rho\,V S\,l_2^2$
C_{mq}	Derivative coefficient of pitching moment due to angular velocity about the pitch axis non-dimensionalised on $\rho\,V S\,l_1^2$
$C_{np}\,C_{nr}$	Derivative coefficients of yawing moments due respectively to roll rate and angular velocity about the yaw axes, non-dimensionalised on $\rho\,V S\,l_2^2$
C_{Yp}	Derivative coefficient of side force due to roll rate non-dimensionalised on $\rho\,V\,S\,s$
$C_{m\dot{w}}$	Derivative coefficient of pitching moment due to acceleration in pitch
$C_{n\dot{r}}$	Derivative coefficient of yawing moment due to acceleration in yaw
g	Acceleration due to gravity
h	Tunnel height (457 mm 18·0 in)
$I_{XX}\,I_{YY}\,I_{ZZ}$	Moments of inertia about the body axes
I_{XZ}	Product of inertia
L	Aerodynamic rolling moment
l_1, l_2	Aircraft reference lengths, *viz.* wing root chord and semi-span respectively
M	Mach number
M	Aerodynamic pitching moment
m	Aircraft mass
N	Aerodynamic yawing moment
$n_1\,n_2\,n_3$	Direction cosines of the body axes relative to the vertical earth axis
$0xyz$	Body datum axes
p	Angular velocity component of the aircraft about the Ox body axis
q	Angular velocity component of the aircraft about the Oy body axis
q	Dynamic pressure ($\frac{1}{2}\rho\,V^2$)
r	Angular velocity component of the aircraft about the Oz body axis
Re	Reynolds' number based on c
S	Aircraft reference area

10

s	Model gross wing area ($0{\cdot}024724$ m^2 $38{\cdot}925$ in^2)
T_x T_z	Components of engine thrust along the datum body axes
u	Translational velocity component along the Ox body axis
$\bar{u}$	u/V
V	Relative wind velocity
v	Translational velocity component along the Oy body axis
$\bar{v}$	v/V
w	Translational velocity component along the Oz body axis
$\bar{w}$	w/V
X	Aerodynamic axial force
Y	Aerodynamic side force
Z	Aerodynamic normal force
α	Incidence angle between the relative wind and the Ox body axis
$\Delta\alpha$	'Lift effect' incidence correction
δ δ'	Tunnel constraint factors
η	Elevon angle relative to Ox body axis
ρ	Air density
NOTE	All forces, moments and associated coefficients are referred to body datum axes.

_____

REFERENCES

No.	*Author(s)*	*Title, etc.*
1	P. L. Bisgood and C. O. O'Leary	Interim report on low speed flight tests of a slender wing research aircraft (Handley-Page HP 115). A.R.C. C.P. 838 (1963)
2	D. W. Partridge	The digital computing system of a wind tunnel flight dynamics simulator. R.A.E. Technical Report 69016 (1969) A.R.C. 31357
3	P. B. E. Engler and G. F. Moss	Low-speed wind-tunnel tests on a 1/8 scale model of the Handley-Page HP 115. A.R.C. R. & M. 3486 (1965).
4	J. S. Thompson, R. A. Fail and J. V. Inglesby	Low-speed wind-tunnel measurements of the oscillatory lateral stability derivatives for a model of a slender aircraft (HP 115) including the effects of frequency parameter. A.R.C. C.P. 1097 (1969).
5	J. S. Thompson and R. A. Fail	Oscillating derivative measurements on sting-mounted wind tunnel models at R.A.E., Bedford. R.A.E. Technical Report 66197 (1966). AGARD CP. 17, p. 437–470.
6	P. D. Smith	Experimental measurement of the ground effect upon a series of eight slender wings. R.A.E. Tech. Memo Aero 1113 (1968).
7	E. C. Maskell	A theory of the blockage effects on bluff bodies and stalled wings in a closed wind tunnel. A.R.C. R. & M. 3400 (1963).
8	Sune B. Berndt	Wind tunnel interference due to lift for delta wings of small aspect ratio. Royal Institute of Technology, Stockholm. Technical Note KTH—Aero TN 19.
9	A. Jean Ross and	An approximate analysis of the non-linear lateral motion of a slender aircraft (HP 115) at low speeds. R.A.E. Technical Report 70 085 (1970). To be published as A.R.C. R. & M. 3674.

APPENDIX A

Normal Force Slope Discrepancy.

In Fig. 7 is shown the difference in slope of some 22 per cent between the normal force results of the present tests and those of Engler and Moss[5] transferred to body datum axes. Further results for $\eta = 0°$ have been obtained by Thompson, Fail and Inglesby[4] using the same tunnel as Engler and Moss but a different, sting mounted, model. In order to compare the slopes from all three results Fig. 17 has been prepared giving results for $\eta = 0°$ in body datum axes derived as follows, *viz*:

Ref. 3 results have been transferred to the appropriate axes using

$$C_z = -C_L \cos \alpha - C_D \sin \alpha.$$

Ref. 4 results have been referred to the appropriate axes by applying an increment of $1\frac{1}{2}°$ to the quoted incidence. The quoted C_z has been applied without any correction associated with this rotation, since there is insufficient data for its computation, and it is certainly extremely small.

Since the results of Ref. 4 are uncorrected for tunnel constraint a further correction to incidence has been made in accordance with Ref. 3. The results from the present tests have been adjusted to $\eta = 0°$ values by subtracting the increments in C_z due to η at various incidences derived from Ref. 3.

Finally all curves have been adjusted by a small increment in C_z to cause them to pass exactly through the origin, so as to clarify the differences in slopes. Taking the Ref. 3 results as datum, Ref. 4 gives 6 per cent more and the present results 22 per cent more.

Possible causes for the discrepancies, *viz.* blockage and constraint effects, model geometrical differences, support differences, Reynolds number effects, are considered below.

Reynolds number.

Ref. 3 has examined Reynolds number effects on C_L over the range $7·86 - 1·17 \times 10^6$ and found them very small. The No. 19 tunnel tests were made at $Re = 2·08 \times 10^6$ and a check was made at $Re = 1·04 \times 10^6$, together with a further check at the higher Re with transition fixed on the wing. Fig. 18 shows the results obtained, transition fixing produced a barely detectable reduction in slope.

Support differences.

The tests of Ref. 3 used a wire rig, whereas the present tests as well as those of Ref. 4 used a sting support. In order to examine sensitivity of the C_z slope to the support geometry a test was made with the sting diameter more than doubled (by application of plasticine and tape). The effect, Fig. 19, was to produce a parallel curve offset by an increment in $\bar{w}$ of 0·01. This type of sting effect has been noted elsewhere and Ref. 6 refers to the routine application of an increment in incidence when using a sting mounting rig.

Geometrical differences.

The principal geometric differences between the simplified No. 19 tunnel model and those of Refs. 3 and 4 are tabulated below.

The effects of the last four differences below have not been examined; the elevon hinge gap might be expected to cause a loss of C_z since Ref. 3 shows that closing the gap significantly affected the C_m/C_z slope.

In Ref. 3 it was found that C_m/C_L was unaffected by closing the intake. Fig. 20 shows measurements of C_z on the present model with fin and nacelle completely removed. Even this drastic modification changed the slope by only about 1 per cent.

So as to examine sensitivity to wing section, the forward facets of the double wedge wing were built up with plasticine and then sprayed with PVC. The leading edge was maintained sharp and the plasticine was blended to the ridge line of the original section. The effect, shown in Fig. 21 was to reduce the C_z

13

Feature	No. 19 tunnel	Ref. 3	Ref. 4
Wing section	Double wedge	Biconvex	Biconvex
Nacelle intake	Conical fairing	Correct, restricted flow	Hemispherical fairing
Rear fuselage	Distorted for sting	Correct	Distorted for sting
Parachute fairing	Omitted	Correct	Correct
Nose probe	Omitted	Correct	Omitted
Elevon gap	Omitted	Correct	Omitted

slope by a little over 7 per cent. The rear facets were then similarly built up to approximate to a biconvex section, and it can be seen in the figure that this made little further difference to the slope but reduced C_{zo} to the Ref. 3 level. Thus some 7 per cent of the discrepancy may be attributable to the use of the simplified wing section of the same thickness :chord ratio.

Blockage and constraint corrections.

The No. 19 tunnel results have been presented, and used in the simulations uncorrected for tunnel effects; the results of Ref. 3 are corrected. The corrections applicable to the No. 19 tunnel results, *viz.* solid blockage, wake blockage, lift effect are discussed below.

Solid blockage.

The correction to kinetic pressure q is given by

$$\frac{q_{cs}}{q} = 1 + 0.65 \frac{V}{h^3}$$

where V is the volume of the model
h is the tunnel height
whence the correction to q is 0·3 per cent.

Wake blockage.

Ref. 3 shows that vortex 'bursting' does not occur until well downstream of the wing trailing edge for all incidences used here; thus from Ref. 7

$$\frac{q_{cw}}{q} = 1 + \frac{1}{2}\frac{S}{h^2} C_{xo}$$

where S is the reference area of the model
whence the correction to q is 0·2 per cent. Thus the slope is in excess by $\frac{1}{2}$ per cent due to neglect of the blockage correction.

Lift effect incidence correction $\Delta\alpha$.

From Ref. 8 for a delta wing in a closed tunnel

$$\Delta\alpha = (\delta + \delta')\frac{S}{C} C_L .$$

14

where δ is a factor dependent on tunnel shape and is 0·137 for a square tunnel; δ' depends on tunnel shape and model chord/tunnel height ratio. C is h^2 for a square tunnel. However in Ref. 3 δ' has not been included in the corrections, so for comparison and since it is considerably smaller than δo it is also appropriate to neglect it here.

Thus

$$\Delta\alpha \doteqdot 0\cdot0165\,C_L.$$

This leads to a slope change of 5 per cent.

It may then be concluded that the combined effects of the section simplification and the neglect of lift-effect constraint could account for the difference between the present results and those of Ref. 4. Since both these results were obtained without the elevon gap being represented it is possible that all three sets of data are consistent.

It should be noted that it is quite feasible to include automatic compensation for any tunnel constraint due to lift in any future flight dynamic simulations at subsonic speeds.

FIG. 1. Handley Page HP 115.

ONE INCH

FIG. 2. HP 115 model.

Cross hatching shows distortions
of the full scale profile

1 in
Scale
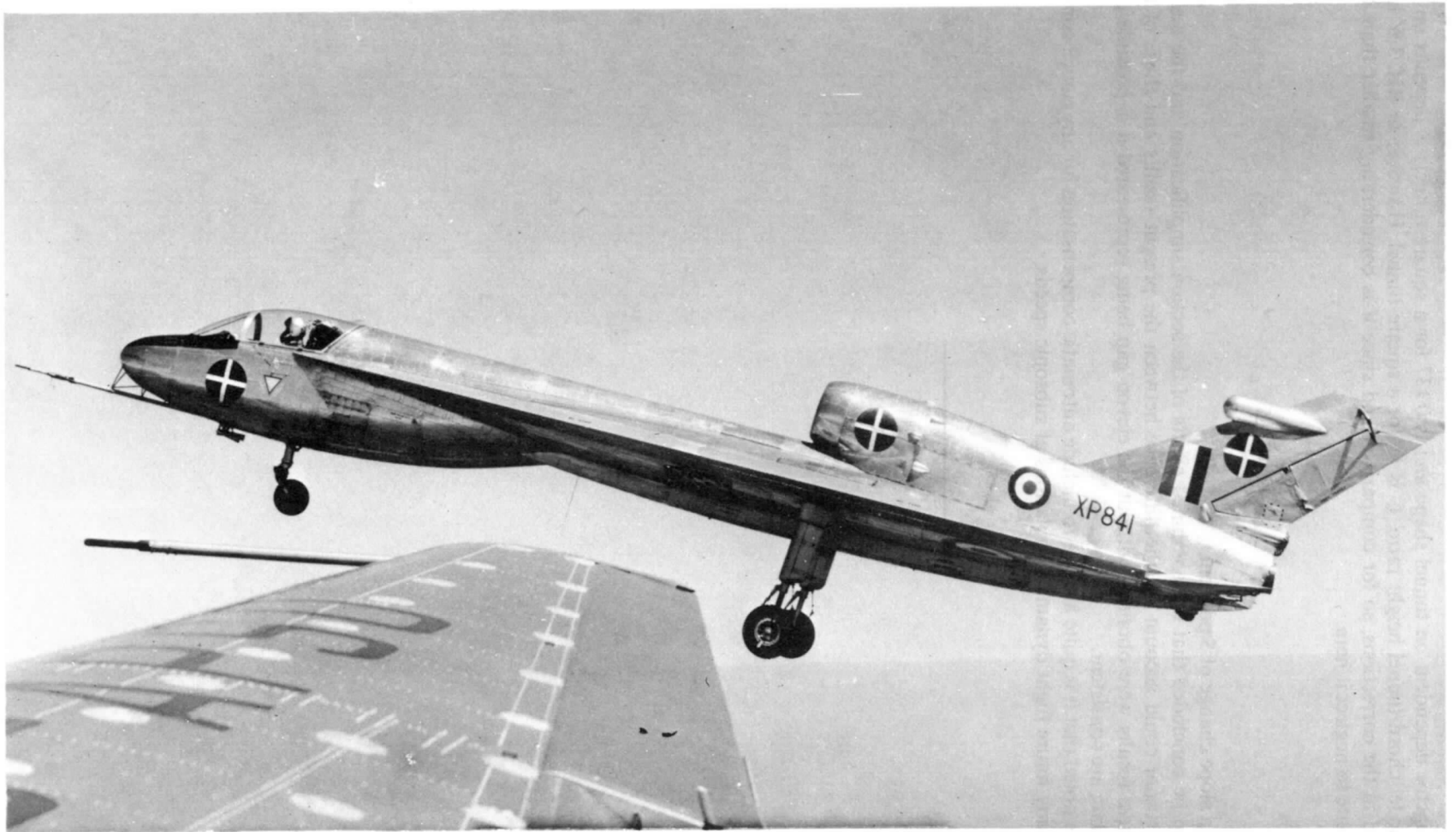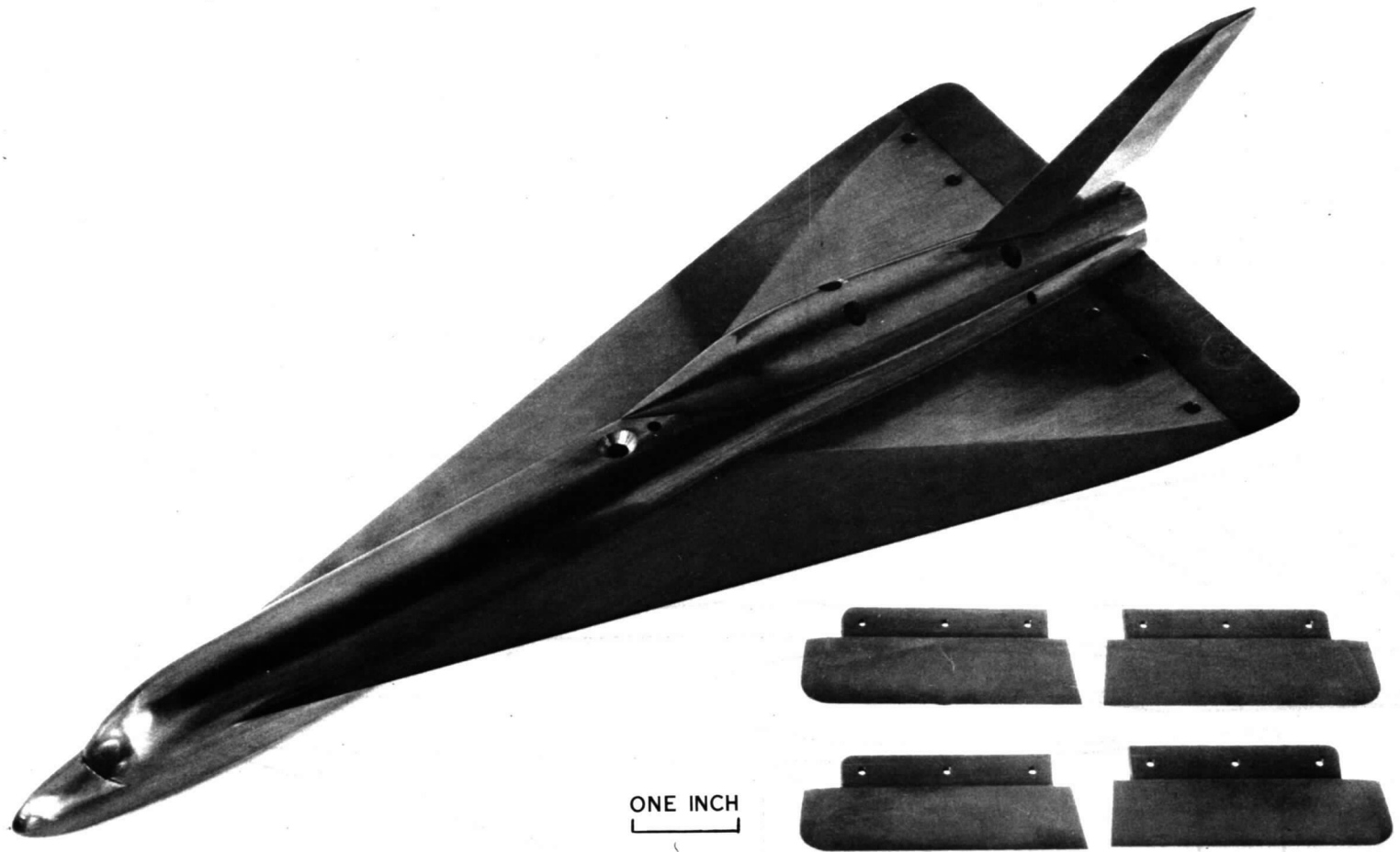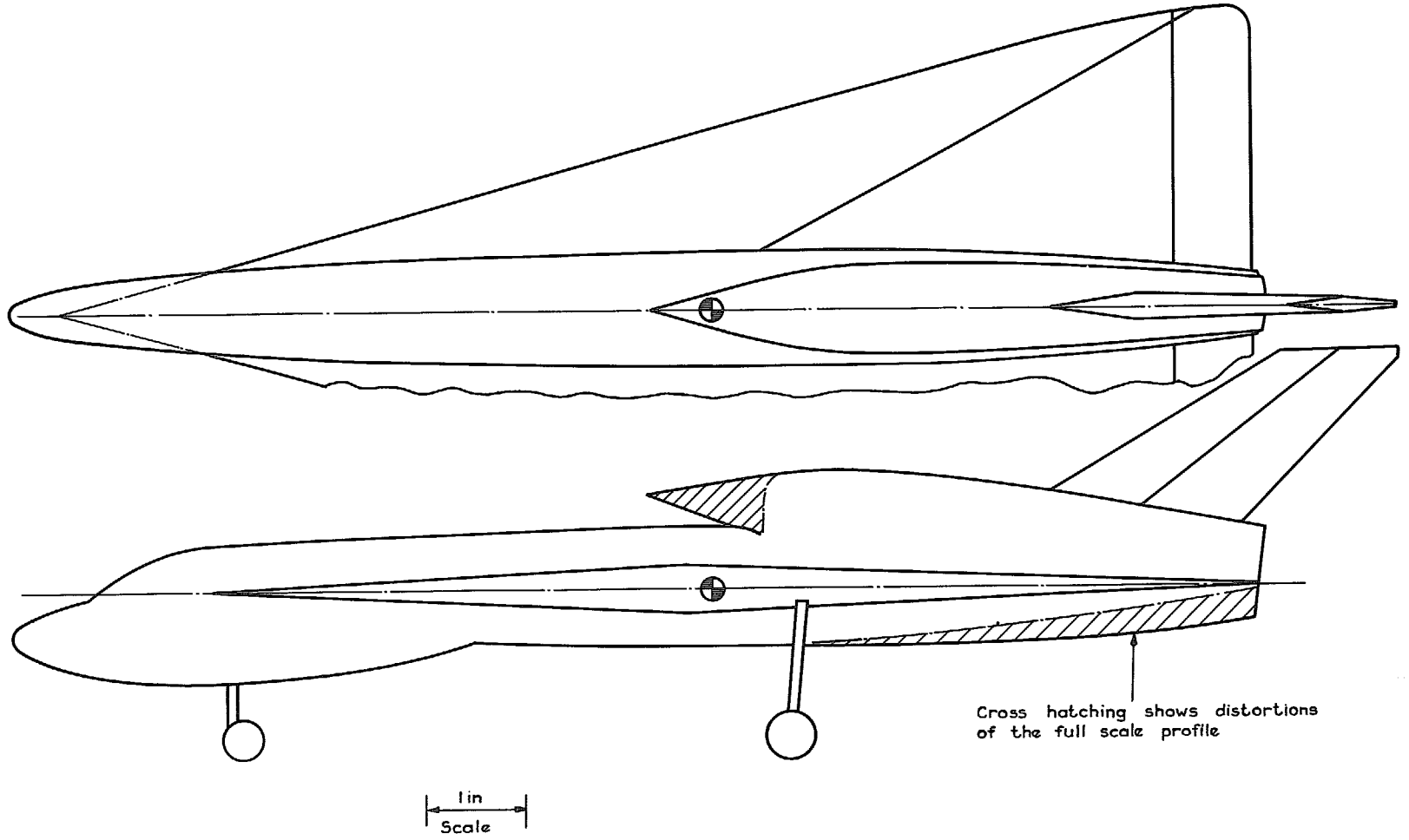
FIG. 3. General arrangement of model.
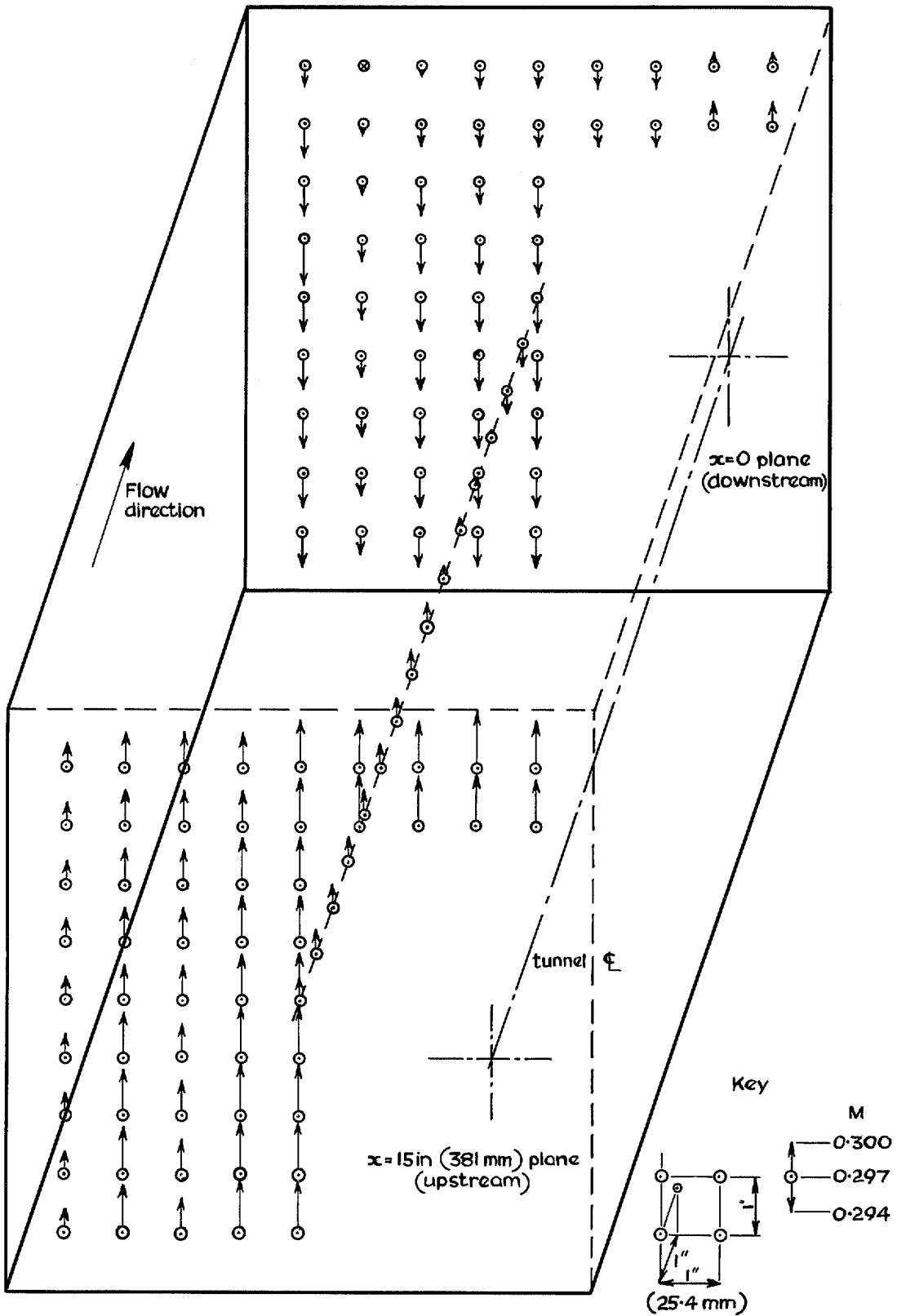
FIG. 4. Mach number distribution.

Flow
direction

X = 7·5 in
(190·5 mm)
plane
(downstream)

Tunnel ₵

X =15 in (381 mm)
plane
(upstream)

Key
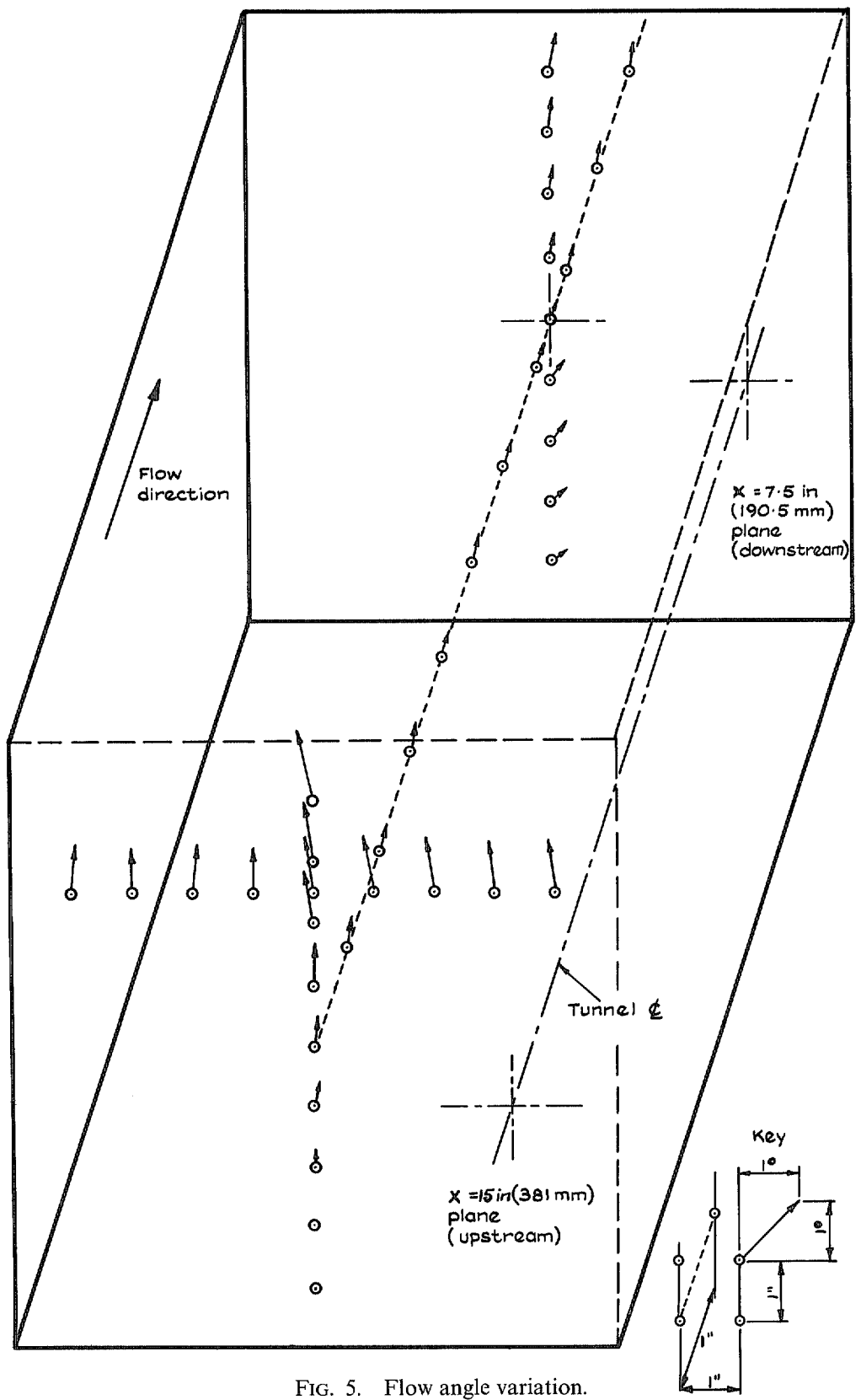
FIG. 5.   Flow angle variation.
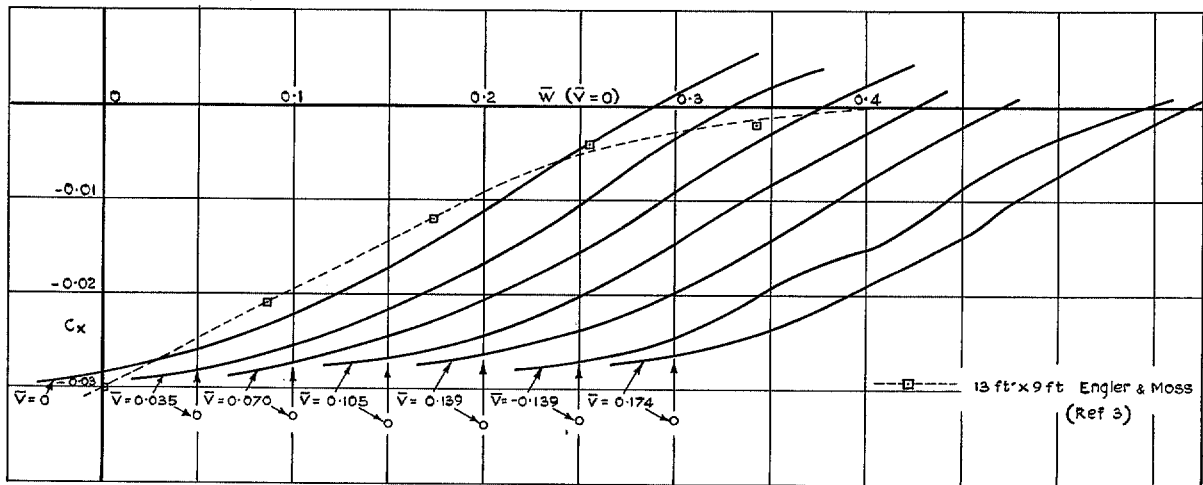
FIG. 6. C_x *vs* $\overline{w}$ at various $\overline{v}$.
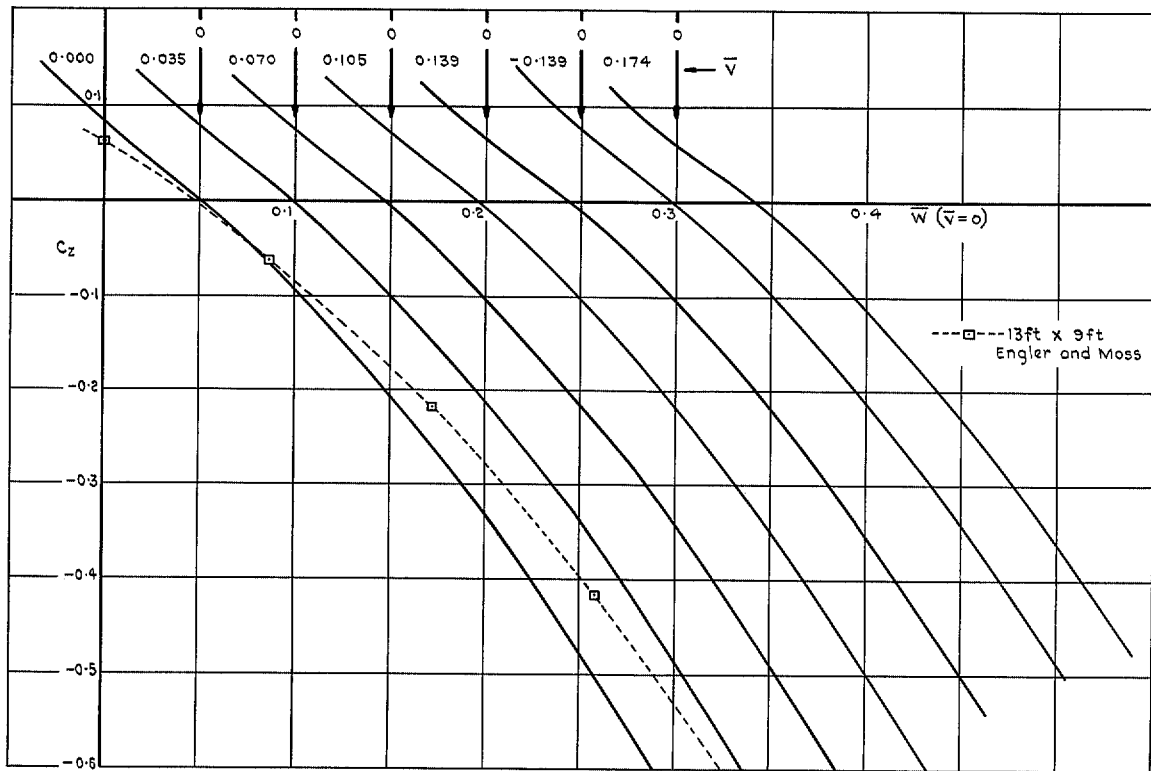
FIG. 7. C_z *vs* $\overline{w}$ at various $\overline{v}$.

21

Cm

0·03

0 0·035 0·070 0·105 0·139 -0·139 0·174 $\overline{V}$

0·02

0·01

0·1 0·2 0·3 0·4 0·5 $\overline{w}$ ($\overline{V}=0$)

-----□---- 13ft × 9ft Engler and Moss

-0·01

-0·02

FIG. 8.   *Cm vs $\overline{w}$ at various $\overline{v}$.*

$\overline{W}$→0·30 0·25 0·20 0·15 0·10 0·05 0

0·02 0·05 $\overline{V}$

0·1 $\overline{W}$

0

0·025

0·02 0·05

0·075 --□- 13ft × 9ft Engler and Moss

0·04 0·100

0·125

0·06

0·150

0·175

0·08

0·200

c_y $\overline{V}$

FIG. 9.   *Cy vs $\overline{v}$ and $\overline{w}$.*

22
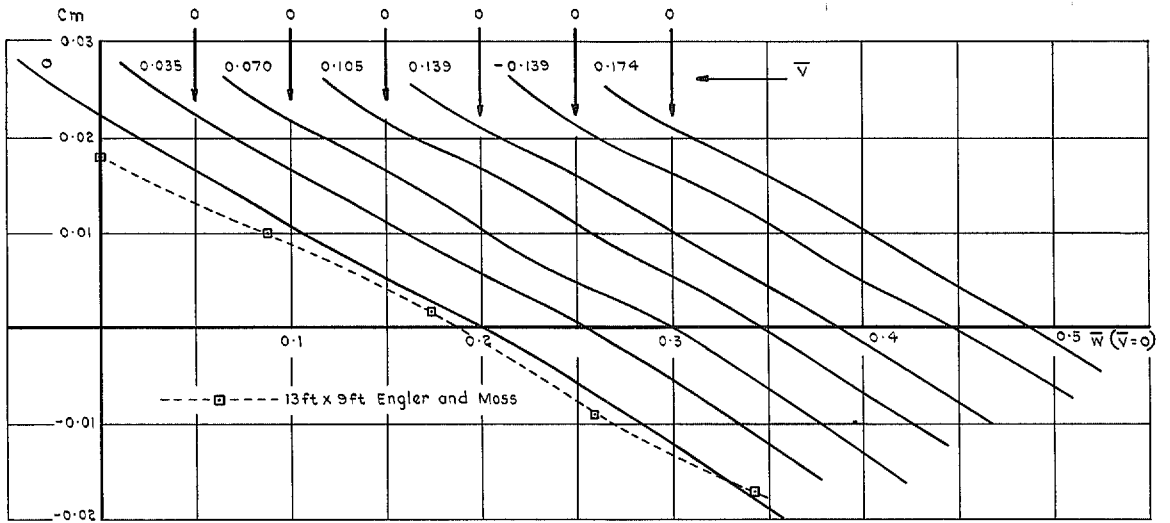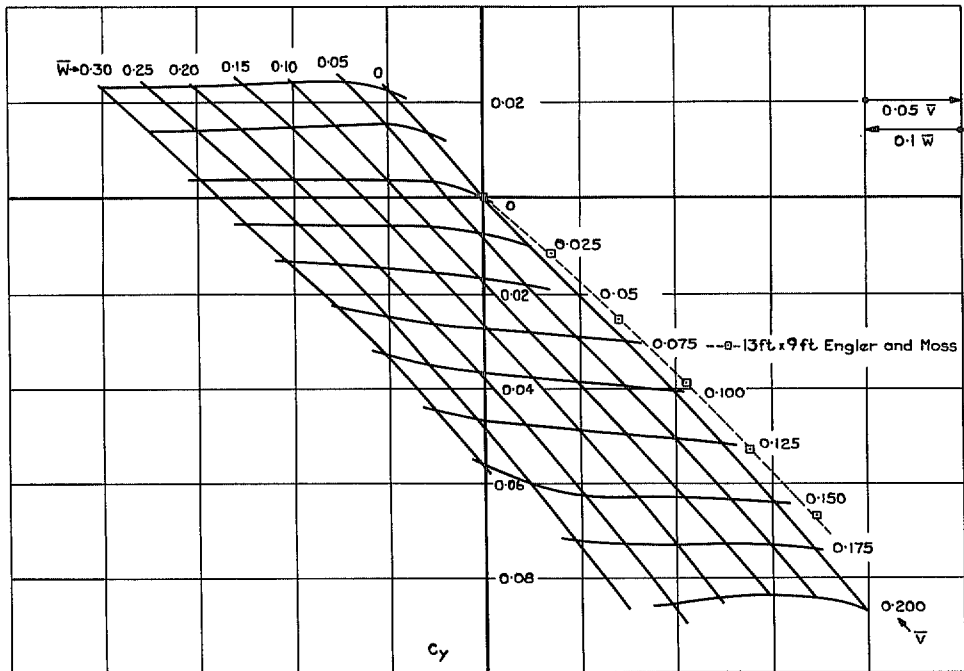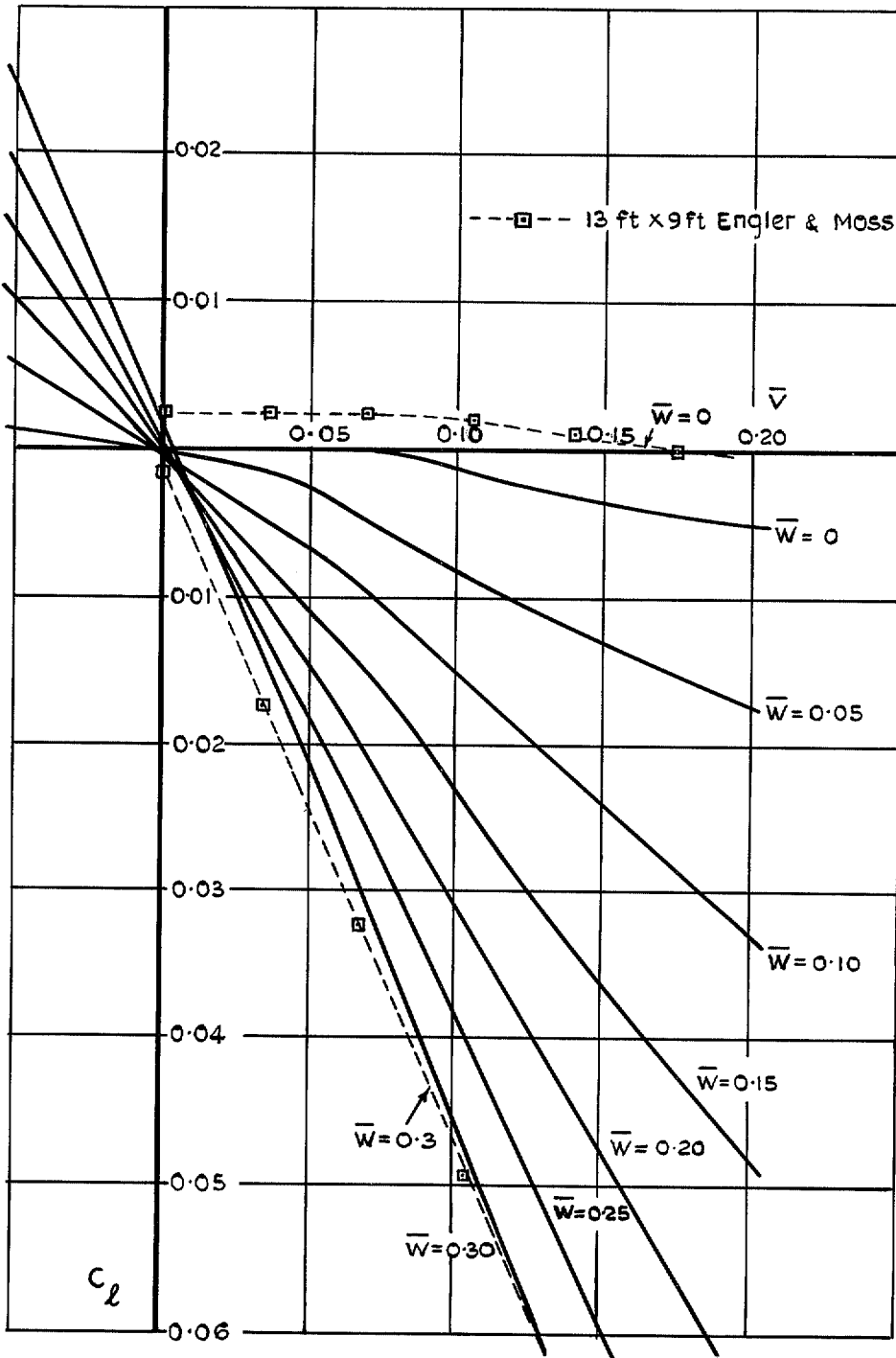
FIG. 10. C_l vs $\bar{v}$ at various $\bar{w}$.
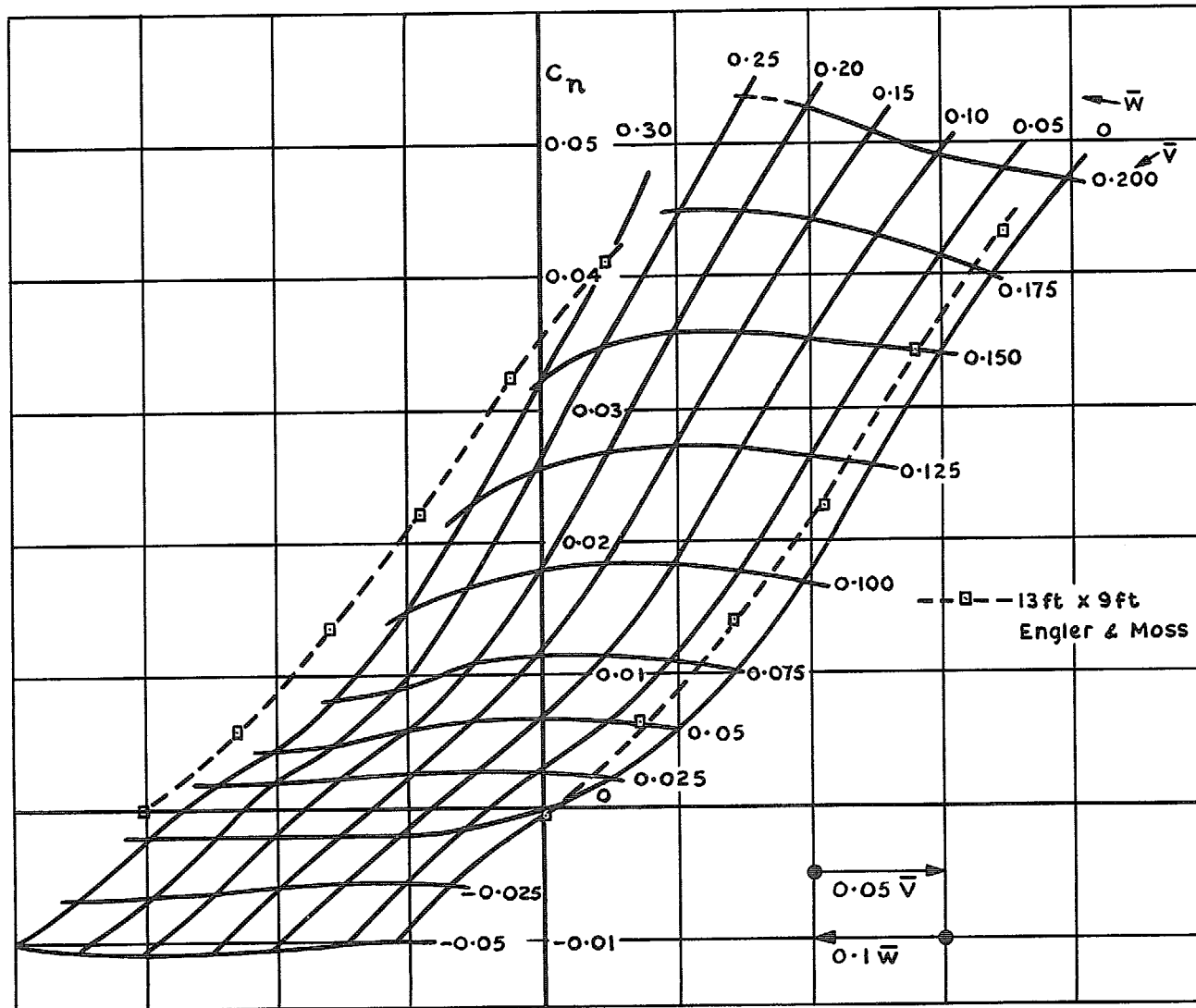
FIG. 11. C_n vs $\overline{V}$ and $\overline{W}$.
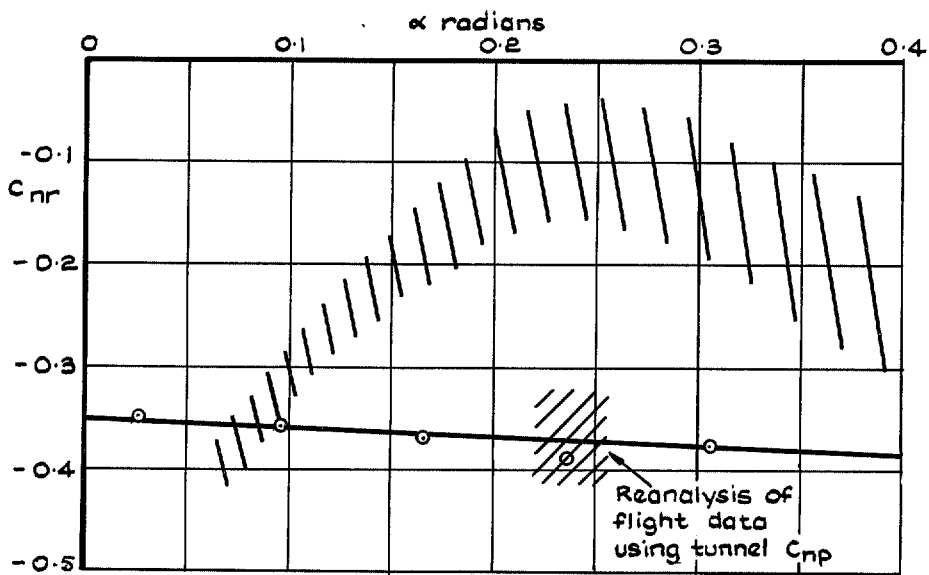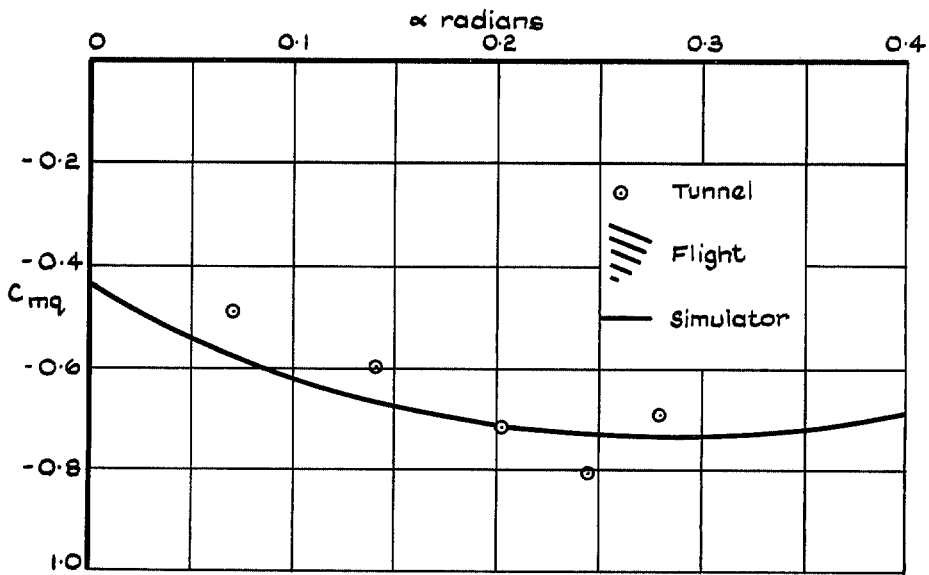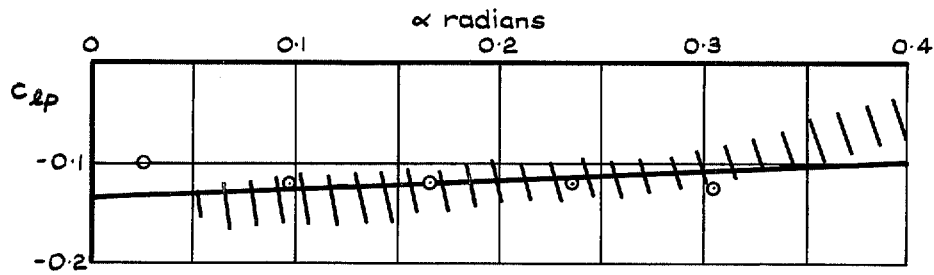
FIG. 12. Dynamic derivatives.

25
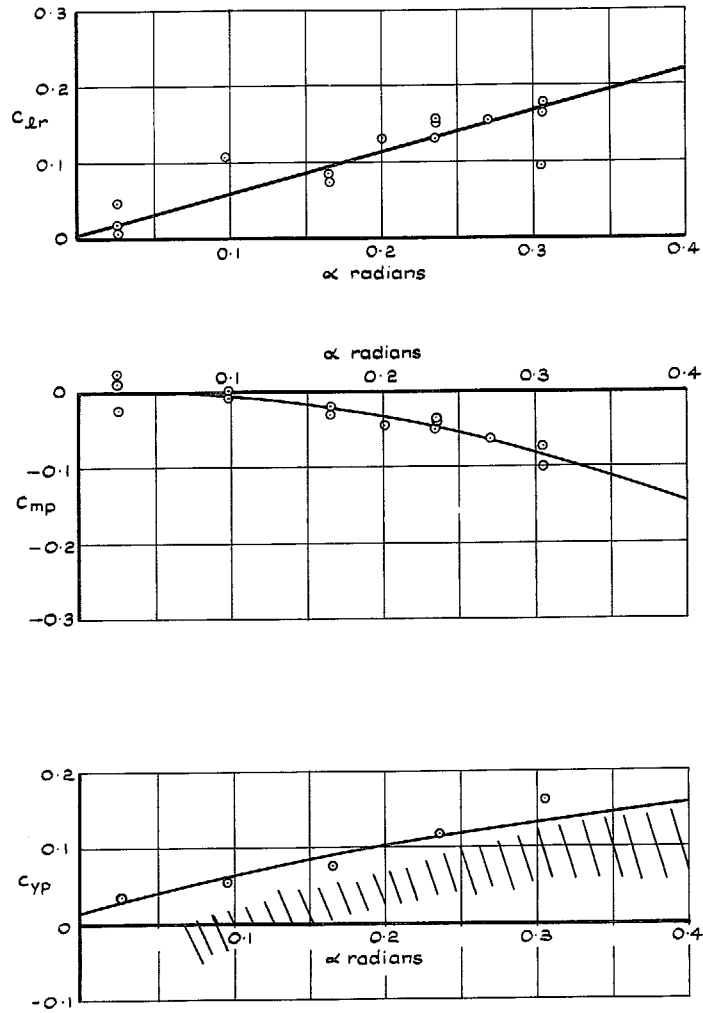
FIG. 12 (contd.)   Dynamic derivatives.

$$\overline{w} = 0.108$$
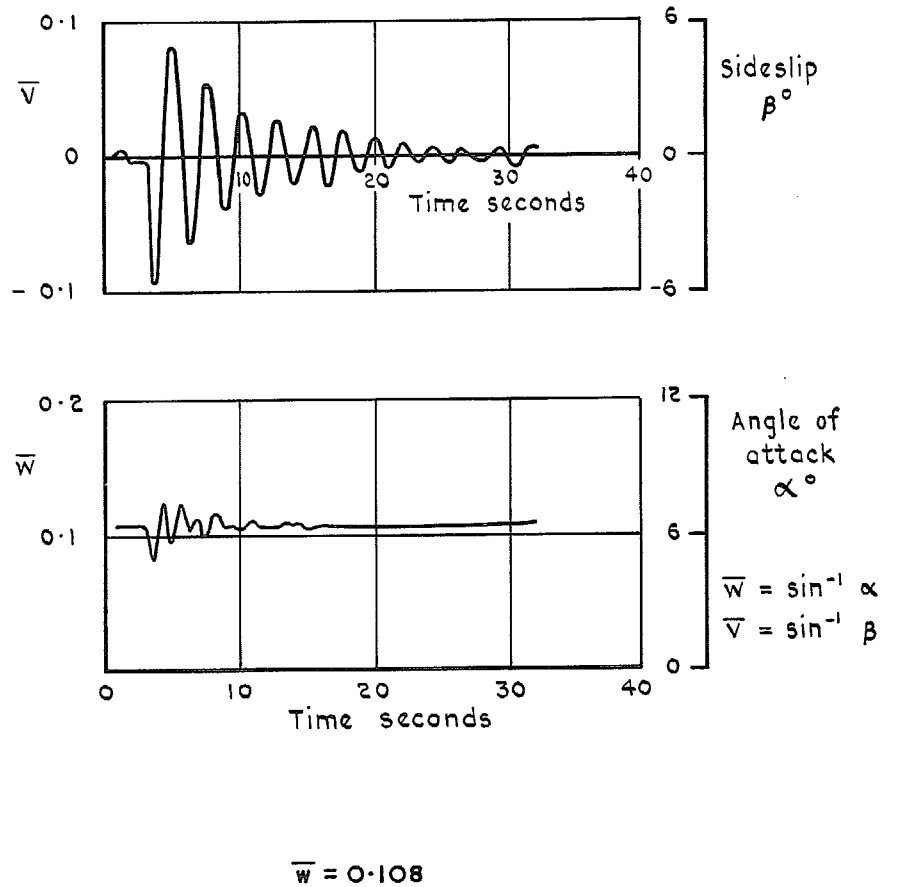
FIG. 13a.   The dependence of the "Dutch Roll" sideslip characteristics $\bar{v}$ on the angle of attack parameter $\bar{w}$.
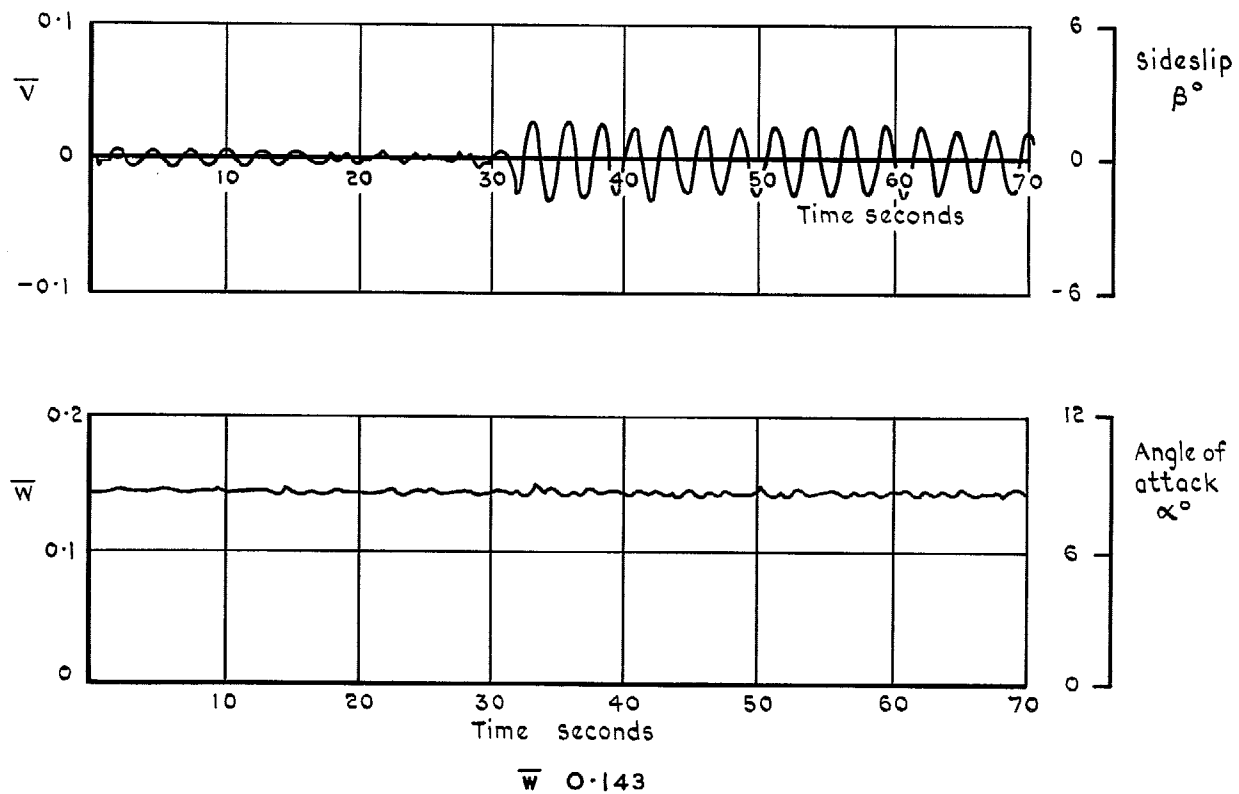
FIG. 13b.   The dependence of the "Dutch Roll" sideslip characteristics $\bar{v}$ on the angle of attack
parameter $\bar{w}$.
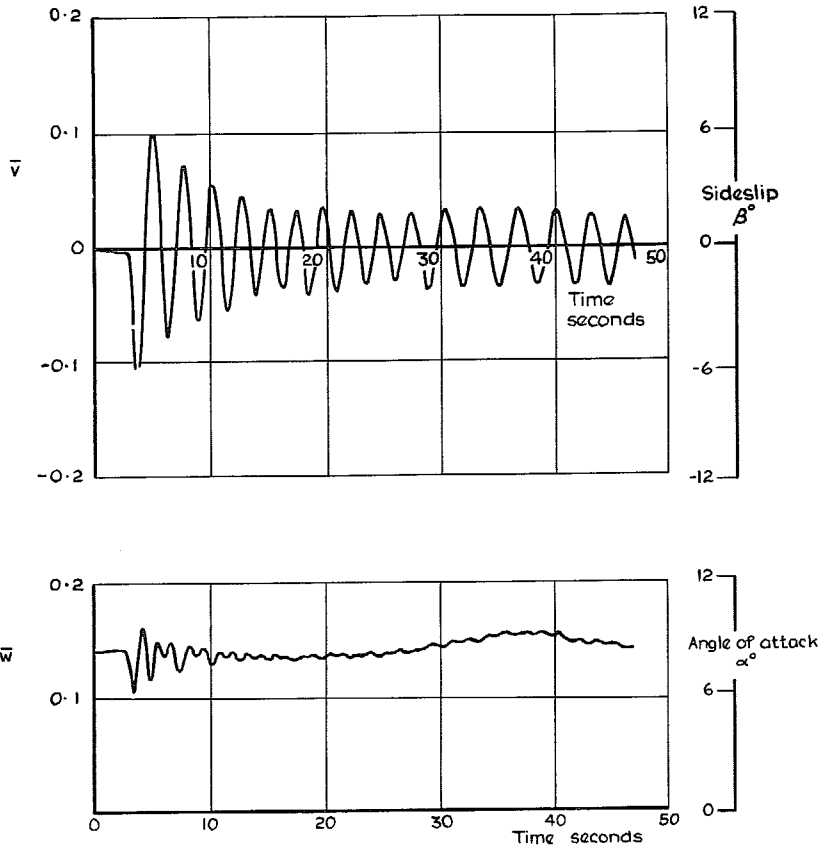
$\bar{w} = 0.14$

FIG. 13c. The dependence of the "Dutch Roll" sideslip characteristics $\bar{v}$ on the angle of attack parameter $\bar{w}$.
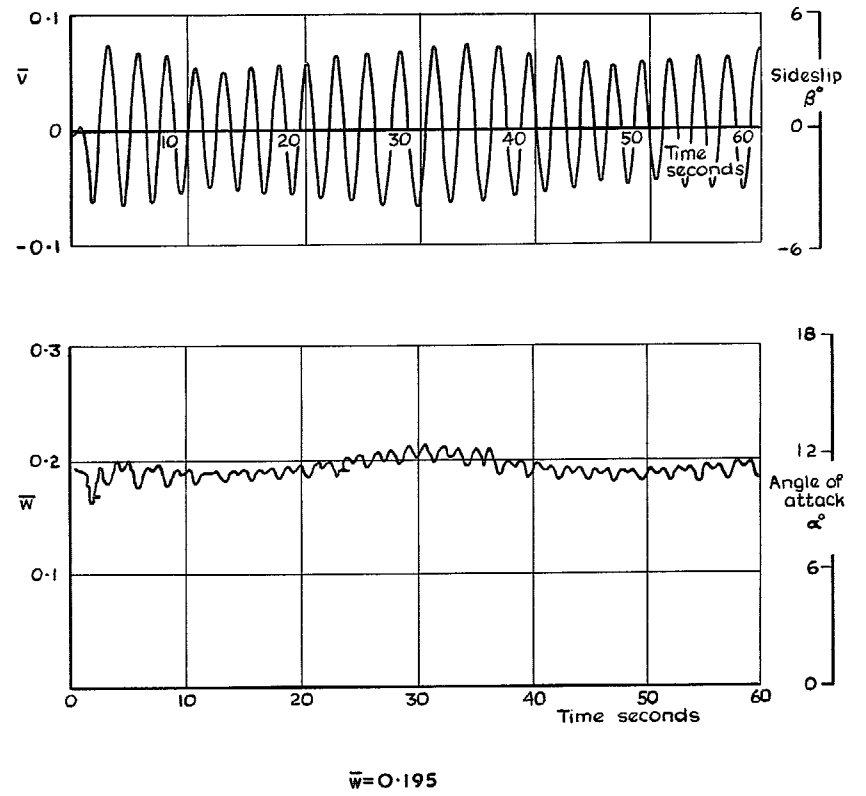
$\bar{w} = 0.195$

FIG. 13d. The dependence of the "Dutch Roll" sideslip characteristics $\bar{v}$ on the angle of attack parameter $\bar{w}$.
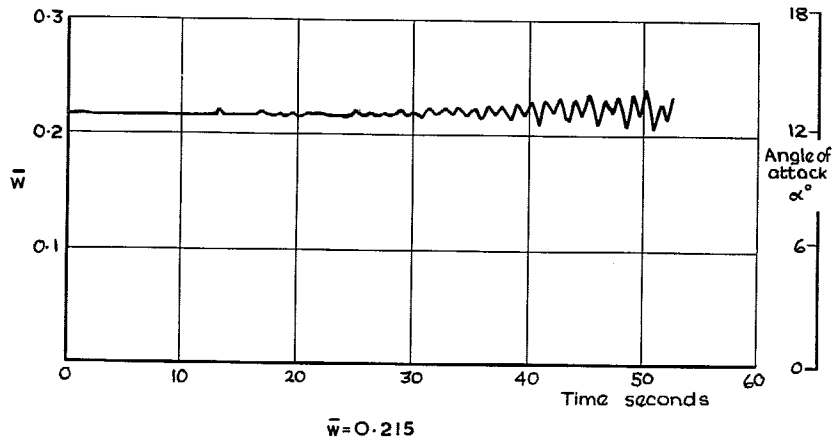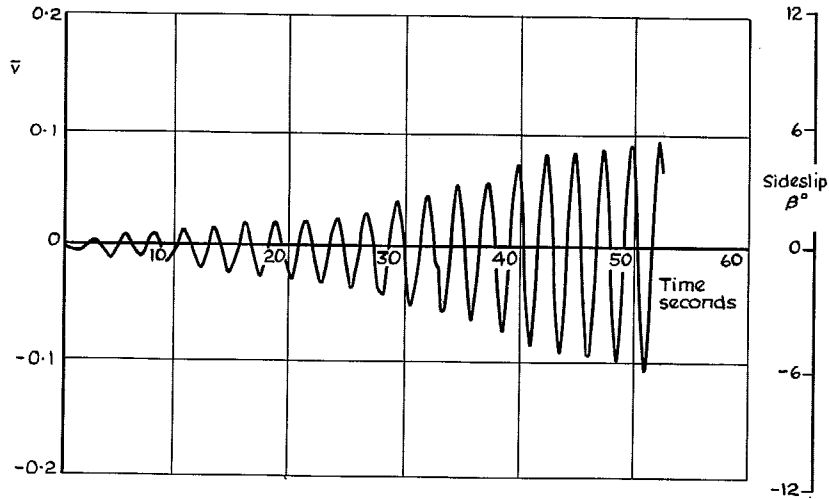
FIG. 13e. The dependence of the "Dutch Roll" sideslip characteristics $\bar{v}$ on the angle of attack parameter $\bar{w}$.
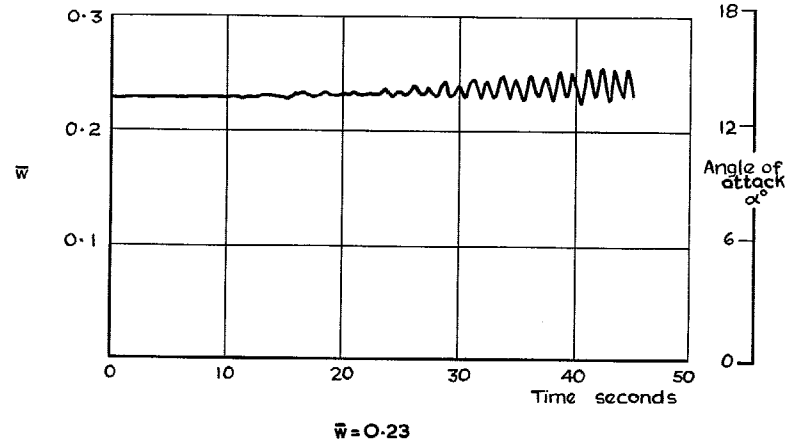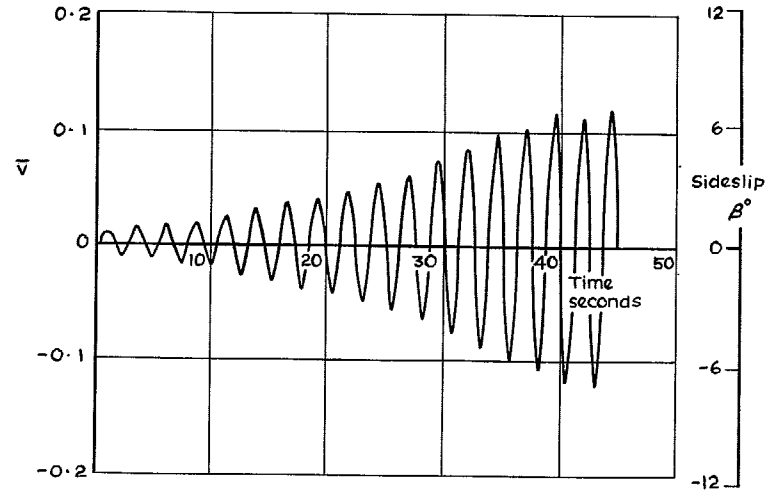
FIG. 13f. The dependence of the "Dutch Roll"sideslip characteristics $\bar{v}$ on the angle of attack parameter $\bar{w}$.
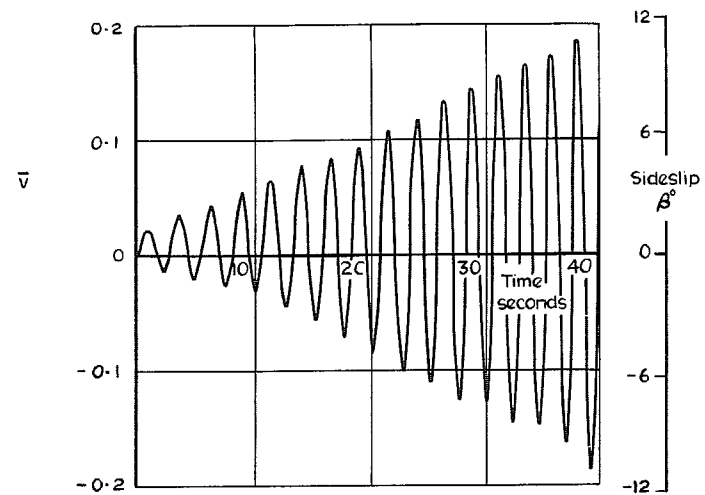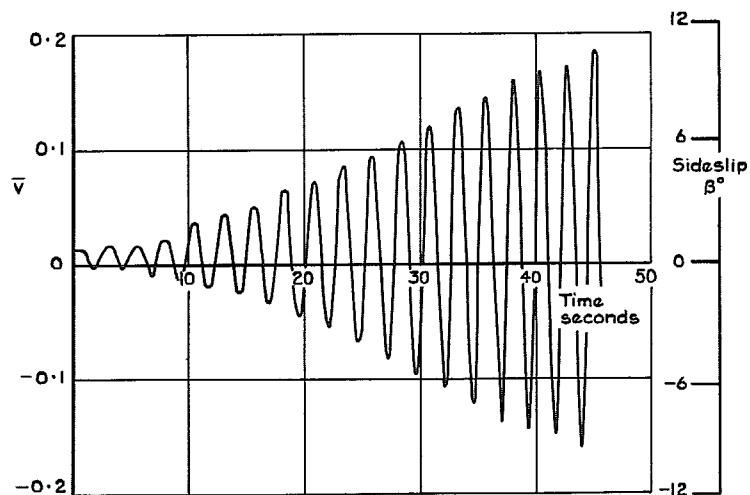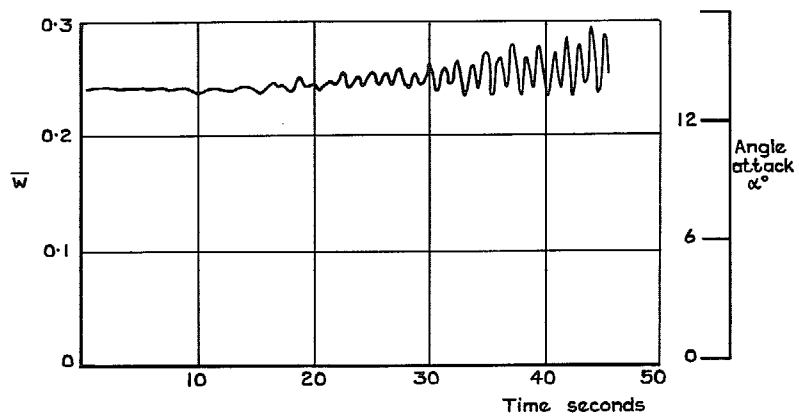
$\overline{w} = 0.24$
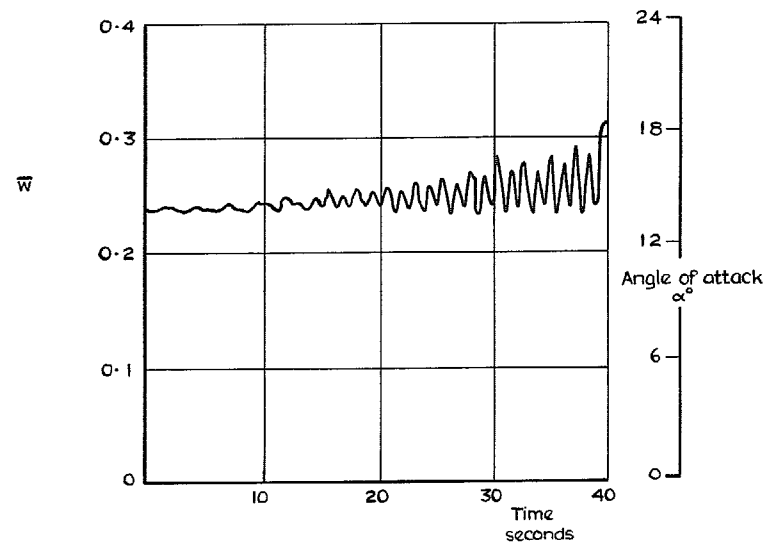
FIG. 13g. The dependence of the "Dutch Roll" sideslip characteristics $\bar{v}$ on the angle of attack parameter $\bar{w}$.

Basic $L(\bar{v}, \bar{w})$

FIG. 14a. Effect of rolling moment magnitude.
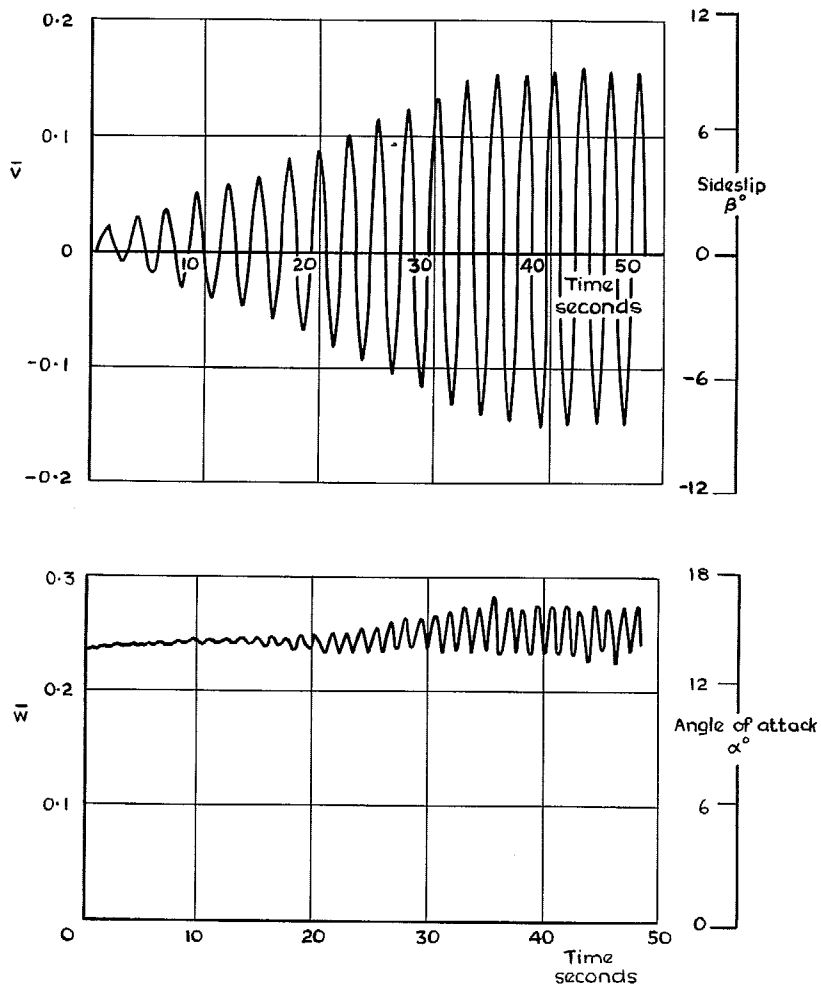
FIG. 14b. Effect of rolling moment magnitude.
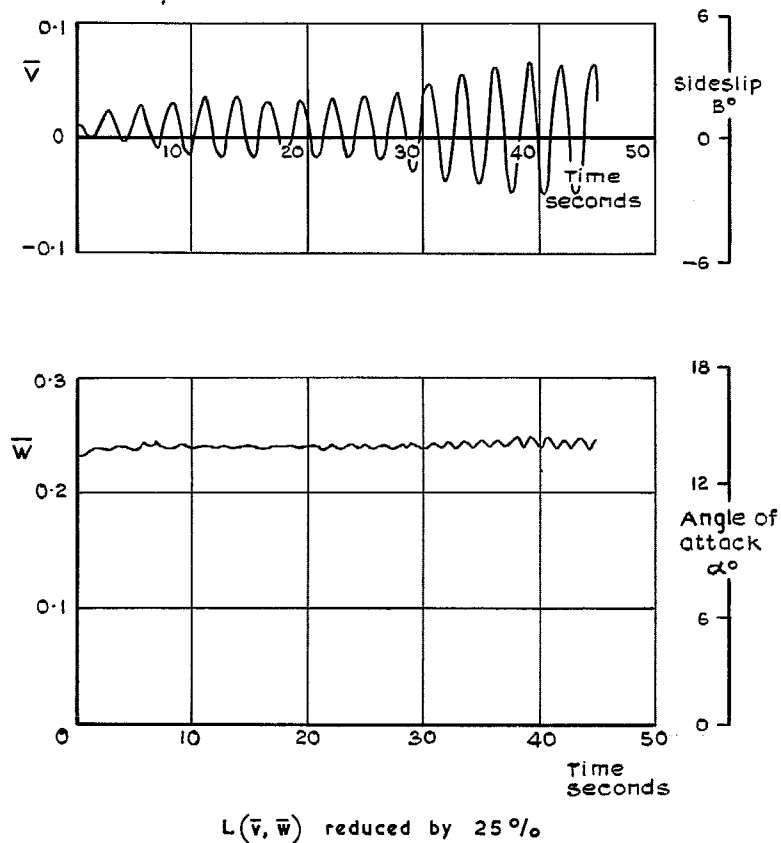
FIG. 14c. Effect of rolling moment magnitude.
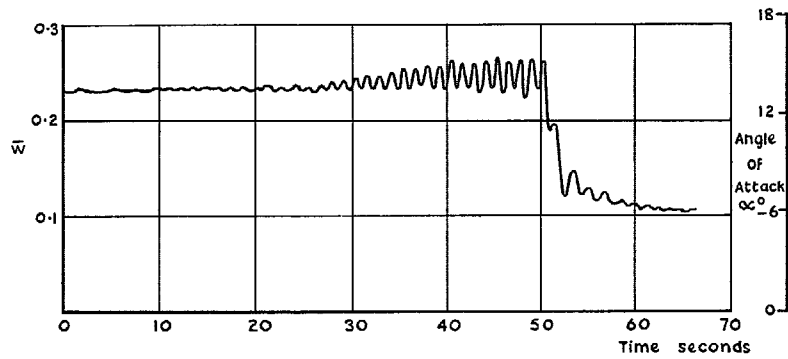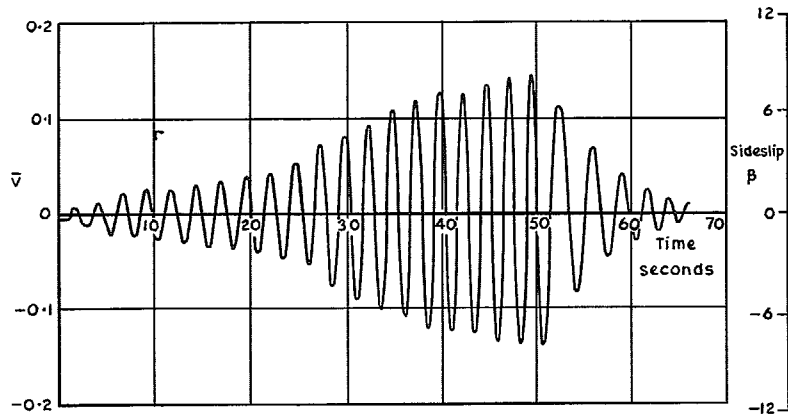
FIG. 15.   Recovery from "Dutch Roll".
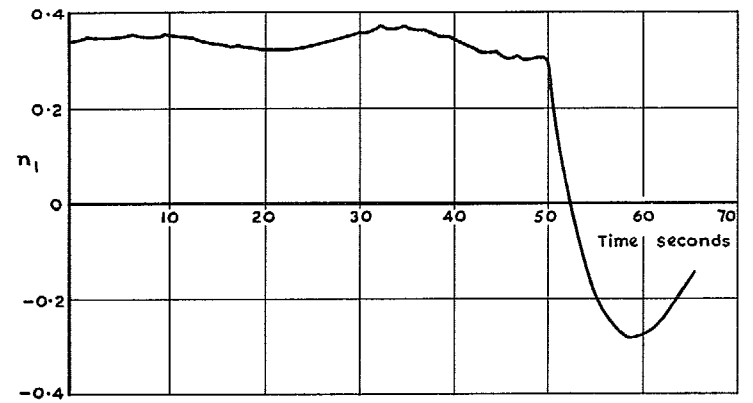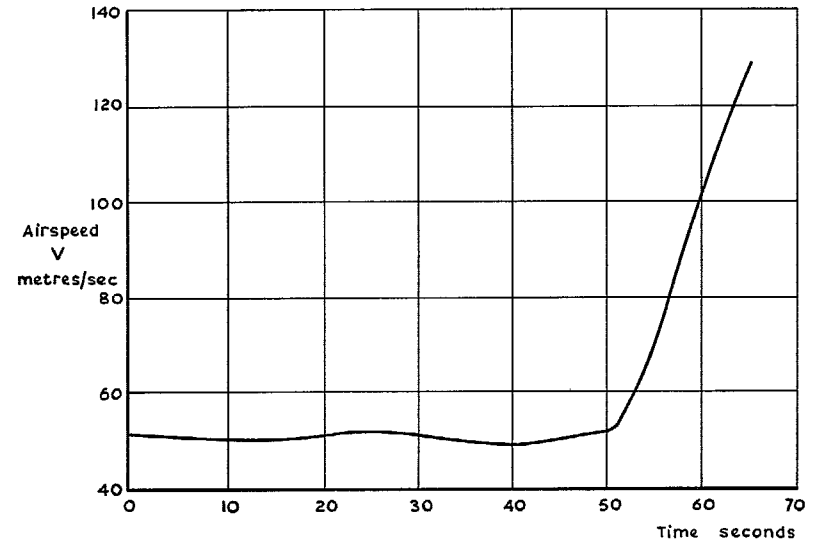
FIG. 15 contd.   Recovery from "Dutch Roll".
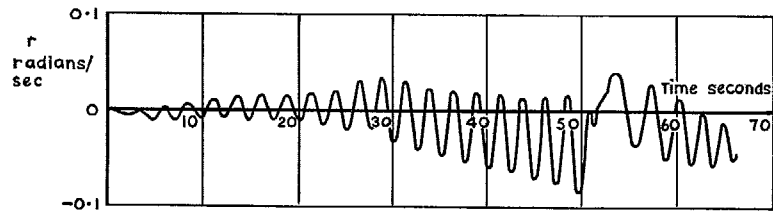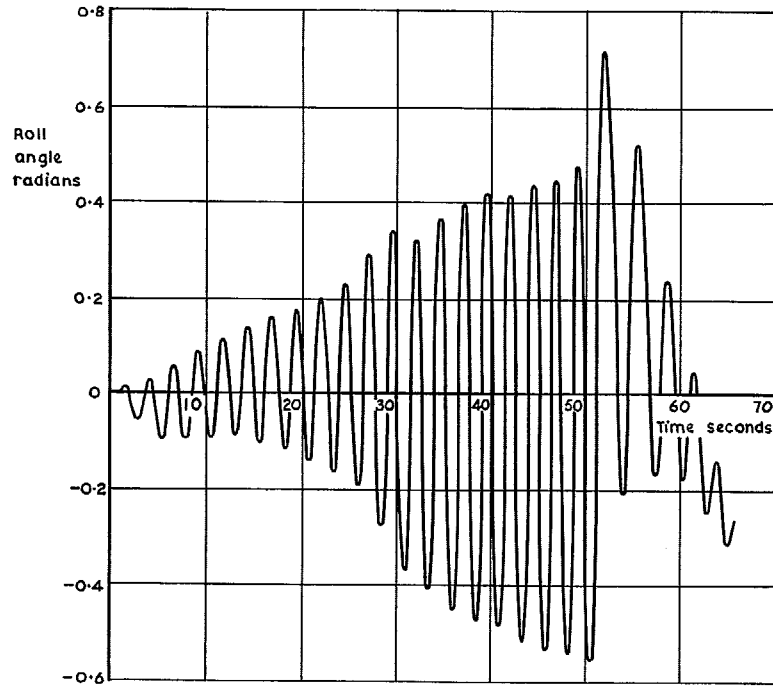
FIG. 15 concld.   Recovery from "Dutch Roll".
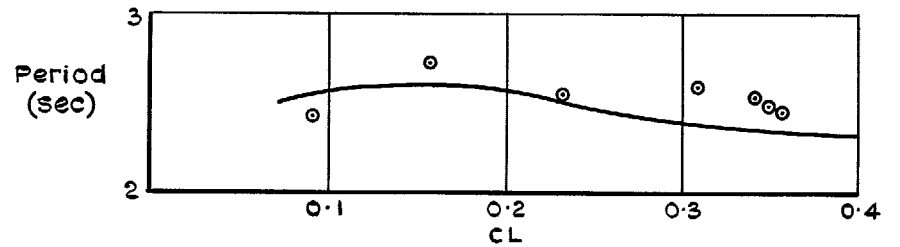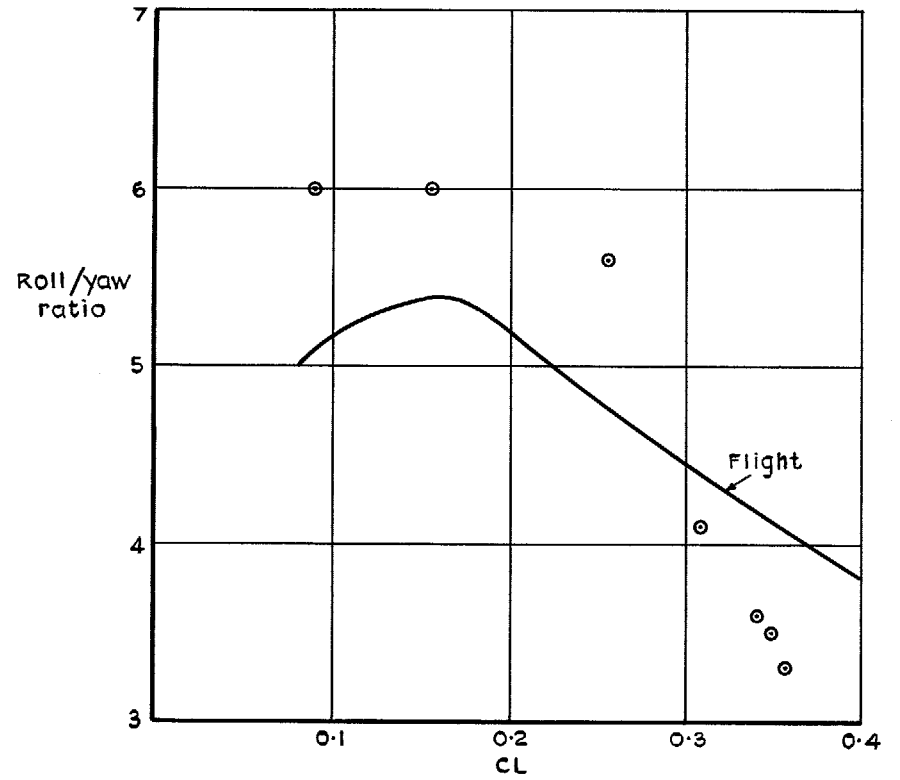
FIG. 16.   Comparison between characteristics of the "Dutch Roll" obtained from the simulator and in flight.
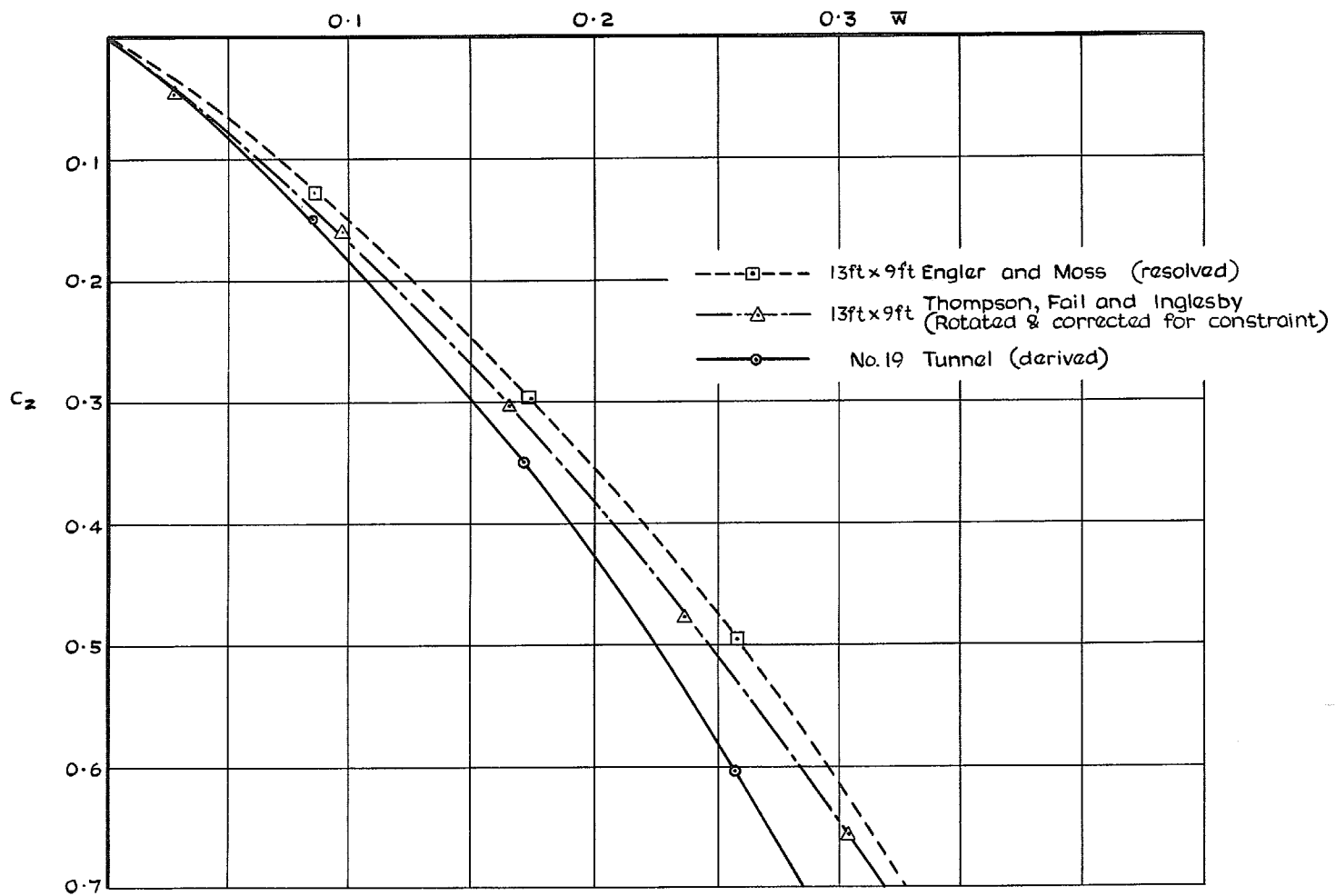
FIG. 17.   Comparison of C_z slope at $\eta = 0°$.
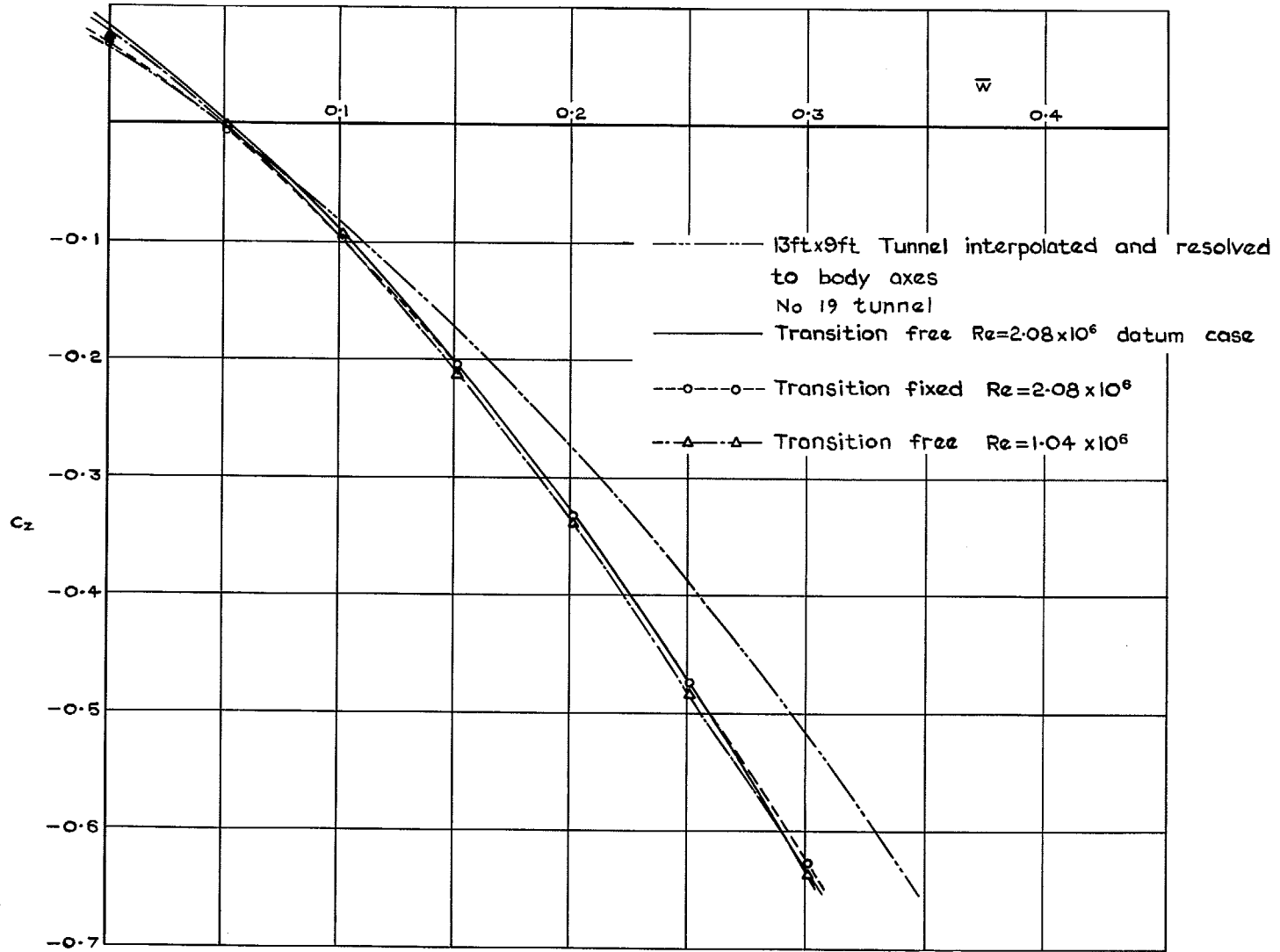
FIG. 18.   Effect of Reynolds number on C_z slope.
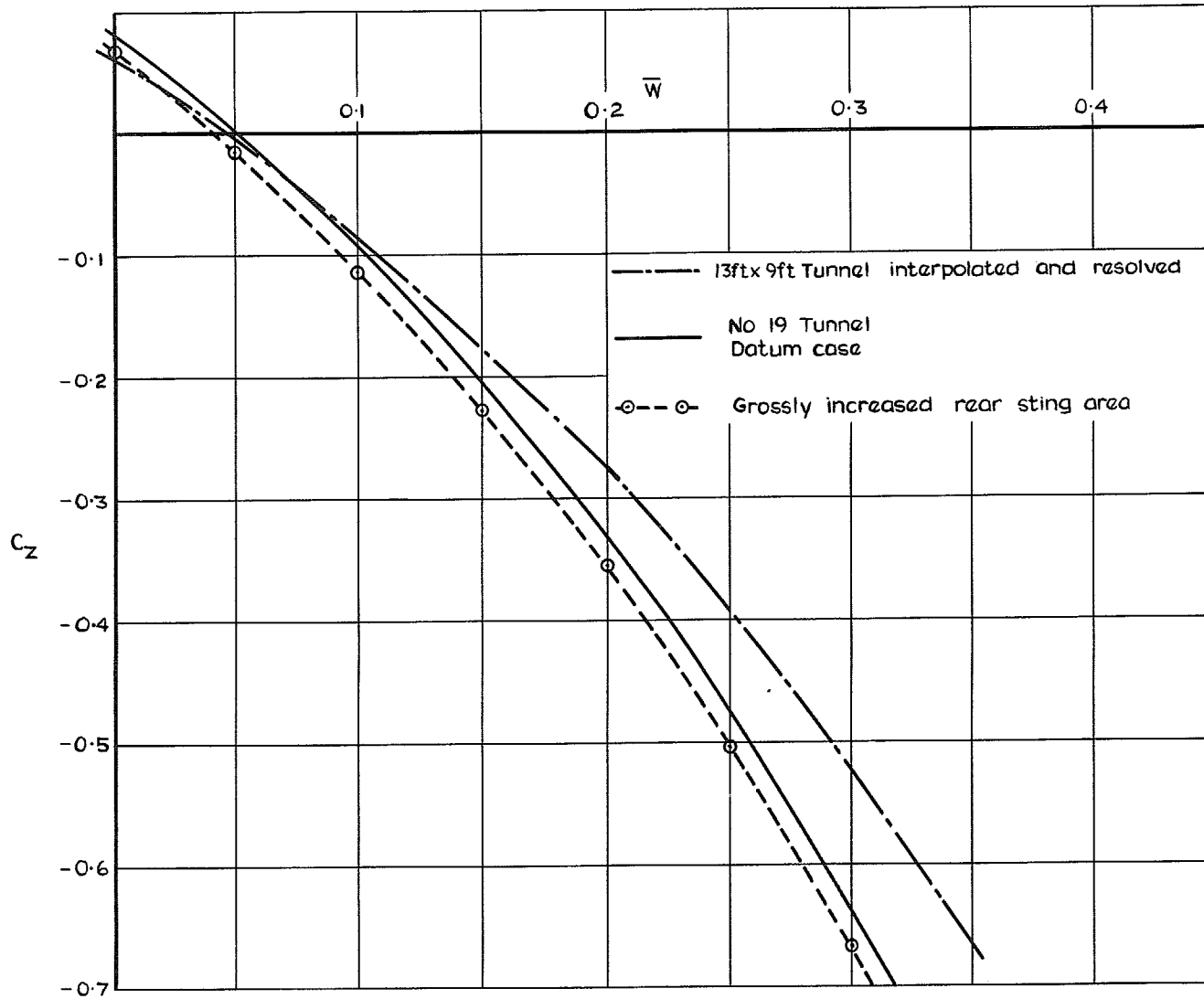
FIG. 19.   Sensitivity of C_z to sting interference.
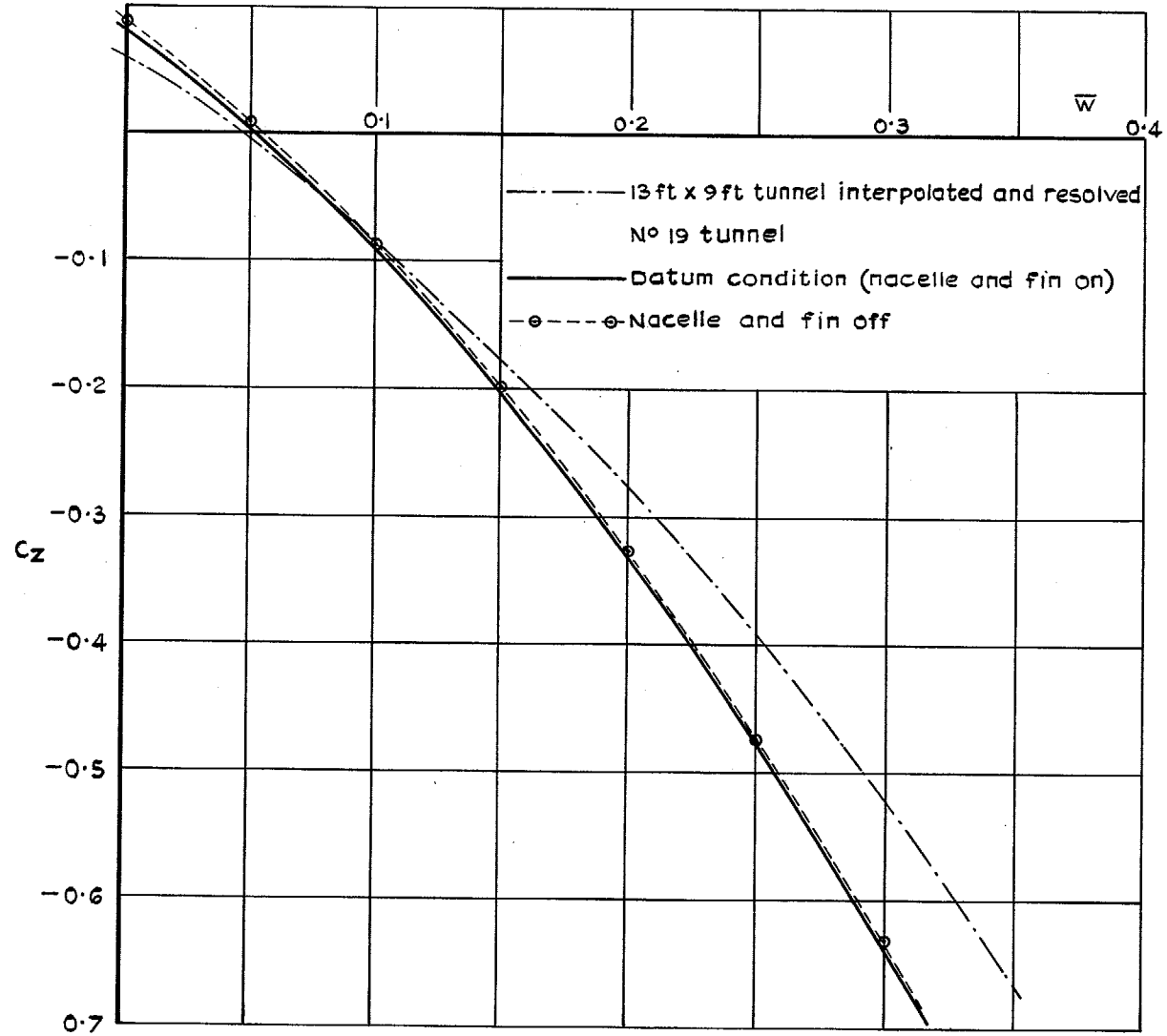
FIG. 20.   Effect of nacelle on C_z.
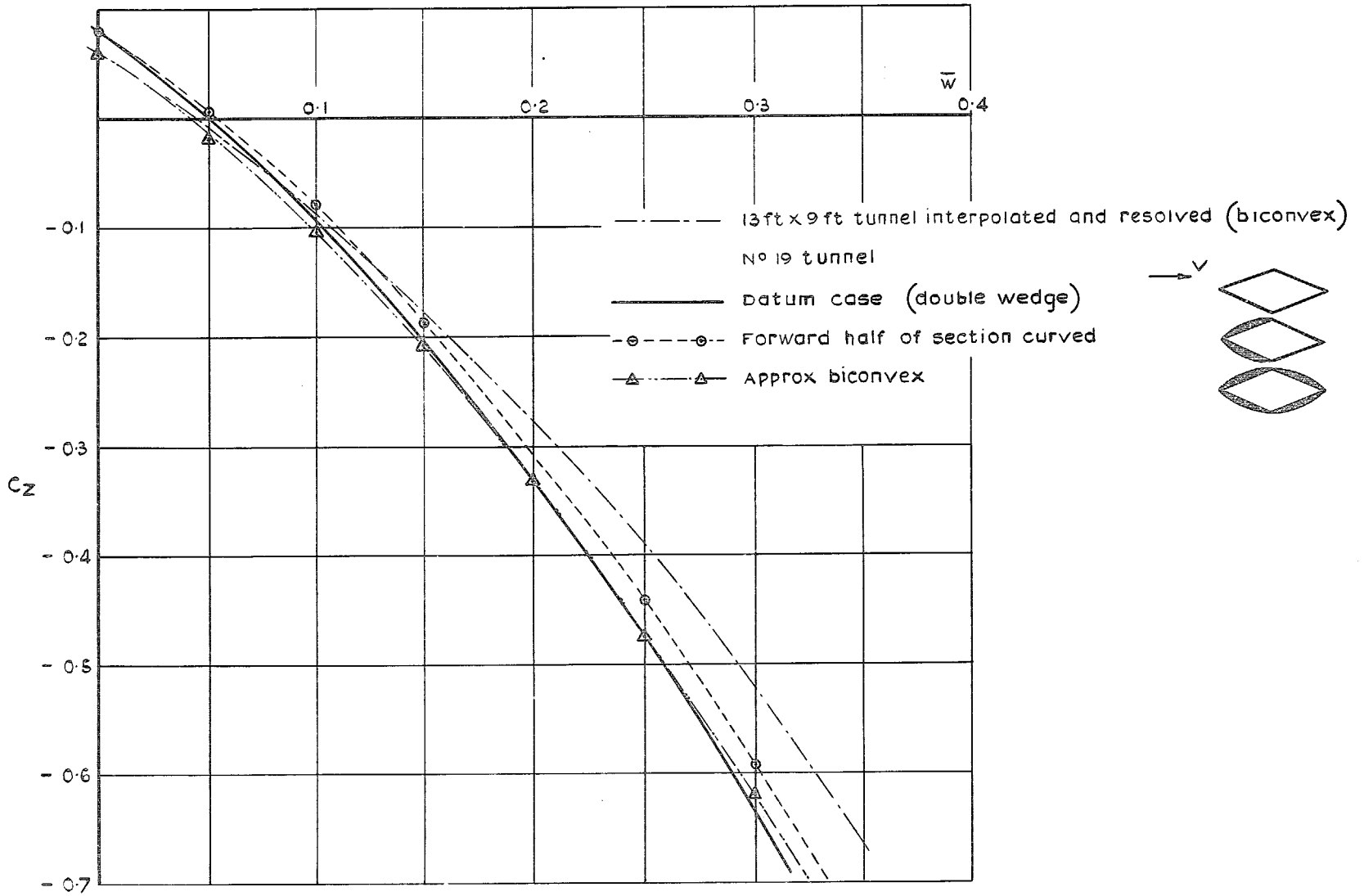
FIG. 21. Effect of wing section on C_z.